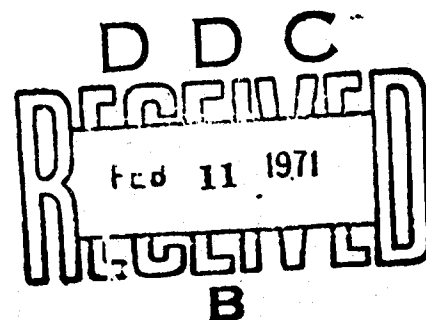DYNAMIC AND STATIC FATIGUE OF SILICATE GLASSES

By

John E. Ritter, Jr. and Charles L. Sherburne

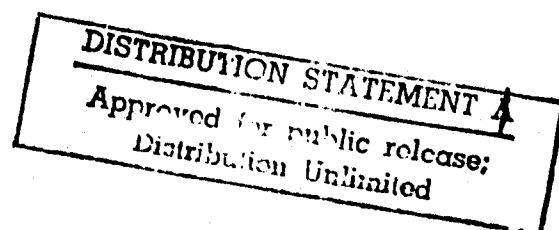Contract No. ONR-NOO.14-68-A-0146-3

Report No. UM-70-9

DISTRIBUTION OF THIS DOCUMENT IS UNLIMITED

D D C

FEB 11 1971

B

December 1970

Approved for Release

Reproduction in whole or in part is permitted for
any purpose of the United States Government. This
research was sponsored by the Office of Naval
Research under ONR Contract No. N00014-68-A-0146,
Subcontract No. N00014-68-A-0146-3, ONR Contract
Authority Identification No. NR 200-016.

Charles E. Hutchinson
Contract Co-Manager
University of Massachusetts

ACKNOWLEDGMENT

ABSTRACT

Fatigue of silicate glasses was studied using both static and dynamic tests. Static fatigue data for acid-etched, soda-lime-silica glass determined at 74° F in atmospheres of 50 and 100% relative humidity could be represented by a single universal fatigue curve. The UFC for acid-etched glass does not lie on the UFC of Mould and Southwick which was determined for aoraded soda-lime-silica glass; the acid-etched glass being less susceptible to static fatigue. On comparing the fatigue behavior of acid-etched, soda-lime-silica glass to that of pristine E-glass and fused silica fibers, little difference was found in the susceptibility to static fatigue. In addition, dynamic fatigue data for a wide variety of silicate glasses (soda-lime-silica, E-glass, pyrex, and fused quartz) was compared to fundamental crack velocity data for these glasses utilizing the dynamic fatigue theory of Charles. Agreement was good on both a quantitative and qualitative level. The theoretical implications of these results on static and dynamic fatigue are discussed.

TABLE OF CONTENTS

LIST OF FIGURES

LIST OF TABLES

1.0 INTRODUCTION

An area of great technological importance and scientific in-
terest is the dependence of fracture stress on the time of loading,
known as static fatigue. Glass loaded at a rapid rate or forced
to support a given load for a short period of time is found to be
relatively strong. In contrast, glass is found to be relatively
weak if the loading rate is slow or if the glass is forced to
support a given load for a long time. The main experimental and
theoretical results on static fatigue have been summarized[1,2] and
the dominant belief is that static fatigue results from a stress-
dependent chemical reaction between water vapor and the surface
of the glass that causes a pre-existing flaw to grow to critical
dimensions for spontaneous crack propagation.

The theoretical stress corrosion model of Charles and Hillig[3,4,5]
has been shown to satisfy most of the experimental results on static
fatigue of abraded, low strength glass. However, because of its
potentially high mechanical strength there is an increasing interest
in the use of silicate glasses as a practical load-bearing material
in such structures as deep submersible vehicles.[2] Therefore, it
is important that the fatigue behavior of high strength glass be
well understood on both an experimental and theoretical basis.
By measuring the dependence of strength on stressing rate of abraded
and acid-etched, soda-lime-silica glass, Ritter[6] has established
that the stress corrosion model of Charles[3] correctly predicts the
effect of dynamic loading on both high and low strength soda-lime-

silica glass. Part of the objective of the present study is to extend the experiments of Ritter to test whether or not the stress corrosion model can predict the effect of static loading on acid-etched, soda-lime-silica glass.

While there have been extensive studies on the effect of chemical composition on corrosion behavior,[7] there has been relatively little work done on relating chemical composition to stress corrosion, although it has been shown that the susceptibility to stress corrosion depends on chemical composition.[8] The only extensive work known to the present author is that of Wiederhorn[9,10] who measured slow crack propagation as a function of stress in various silicate glasses by the double cantilever beam technique. Thus, the second phase of the present study is to measure the strain rate sensitivity of various silicate glasses and compare these results to those of Wiederhorn. In this way it is hoped to more clearly elucidate the dependence of stress corrosion susceptibility to chemical composition.

2.0 LITERATURE SURVEY

2.1 Strength of Glass

All theoretical estimates of the strength of glass result in values from 1×10^6 to 5×10^6 psi.[2,11,12] Since the measured strengths of glass articles are in thousands, not millions, of pounds per square inch, Griffith[13] proposed that micro-cracks or small flaws exist at the surface of glass. By equilibrating the rate of decrease of strain energy associated with growth of the flaw under stress to the rate of increase of surface energy, he found that the fracture stress is inversely proportional to the square root of the depth of the surface flaw. Orowan[14] reached the same conclusion through an alternate derivation. Orowan proposed that fracture is due to the stress-concentrating action at the tip of the flaw. Fracture occurs when the applied stress produces a stress at the flaw tip equal to the intrinsic strength of the glass. The observed strength of a glass specimen is thus the applied tensile stress that will initiate crack propagation at the most severe flaw present in the stressed region. Once started, the extension of the crack is ensured by the applied stress and the increasing stress concentration factor of the growing crack. Surface flaws can range from discontinuities of atomic dimensions, with associated strengths in the range of one million psi, to gross mechanical damage that reduces the strength to a few thousand psi. Since the flaws cannot grow under a compressive stress, the flaw concept also accounts for the fact that glass is extremely strong in compression. The

presence of surface flaws is by far the most important single factor
in determining the observed strength of any glass specimen.

2.2 Static Fatigue

When glass supports a load the chemical interaction of at-
mospheric water vapor with the glass surface often leads to a time-
dependent reduction in strength, known as static fatigue or delayed
failure. Excellent reviews of the subject have been written by
several authors.[11,12,15-17] It is generally believed that static
fatigue results from a stress-dependent chemical reaction between
water vapor and the glass surface which causes an alteration in the
shape and/or depth of surface flaws. The rate of the reaction is
thought to increase with the state of stress at the surface, the rate
increasing with increasing stress. Because of the stress concentra-
tion effect, the chemical reaction proceeds more rapidly from the
tips of surface cracks, and since the reaction products are weaker
than the unreacted glass, the cracks lengthen with time. Failure
occurs when the crack is sufficiently long to satisfy the Griffith
criterion. That is when the stress at the crack tip increases to
the ultimate cohesive strength of the glass. The time to failure
in a static fatigue test is the time for a surface flaw to grow from
subcritical to critical Griffith size. This time depends on the
magnitude of the applied stress, the duration of exposure to a
reactive environment, and physical parameters characteristic of the
material.

2.3 Fatigue Theory of Charles

Charles[3,4] assumed flaw growth at a constant temperature
may be described by an equation of the form

$$v_x = k\,\sigma_m^{\,n} \tag{1}$$

where v_x = velocity of the flaw tip in the x direction (the direction
of maximum tensile stress gradient), σ_m = normal tensile stress
at the flaw tip and k,n = constants. He derived that for the case
of dynamic fatigue, where an increasing load is applied until failure,
the breaking strength of glass should vary with the rate of stress
application as follows:

$$\sigma_{af} = K\beta^{1/n+1} \tag{2}$$

where σ_{af} = macroscopic applied tensile stress at which failure
occurs, β = rate of stress application, and K = constant.

2.4 The Universal Fatigue Curve of Mould and Southwick

The most comprehensive experimental investigation of static
fatigue was conducted by Mould and Southwick[15] who studied delayed
failure as a function of stress over nine logarithmic decades of time.
Working with soda-lime-silica glass microscope slides subjected to
a variety of surface abrasions, they found that the static fatigue
behavior could be characterized by a single curve, Fig. 1, when
failure times and applied stresses are given in reduced units.
The reduced stress is defined as σ/σ_N where σ_N is the fracture
stress measured at liquid nitrogen temperature. The reduced time
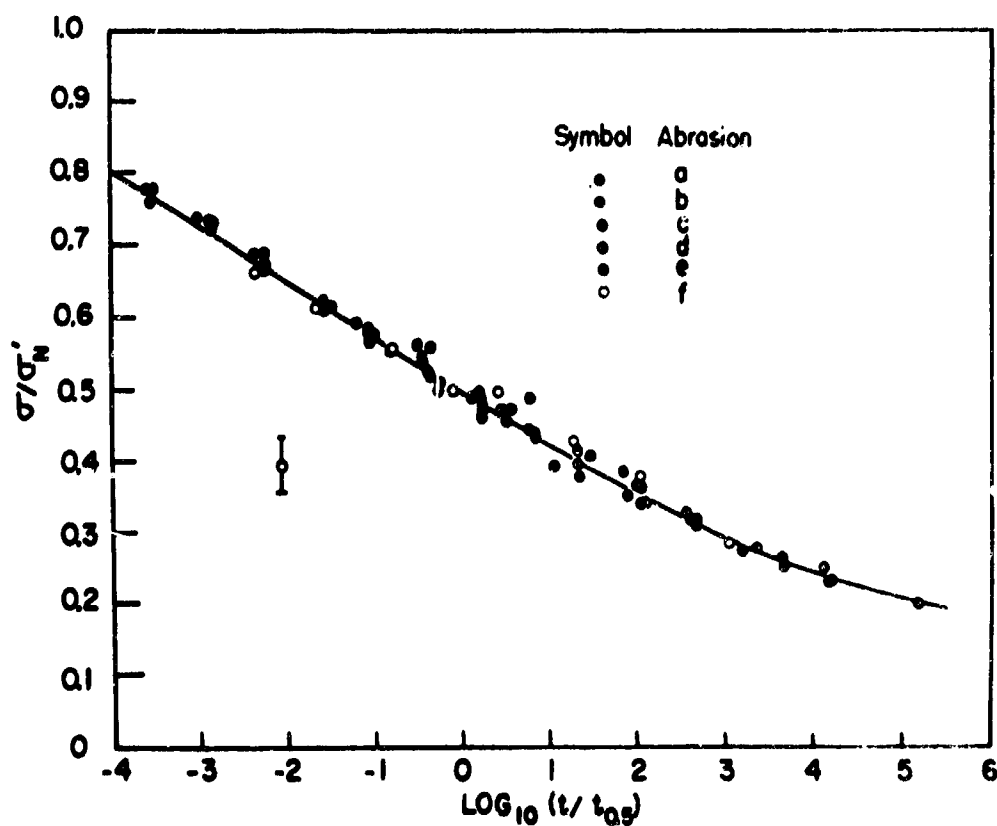
Figure 1. Universal fatigue curve for soda-lime glass abraded in various ways (after Mould and Southwick[15]). σ is the applied stress. σ_N is the fracture stress measured at liquid nitrogen temperatures. t is the delayed failure time. $t_{0.5}$ is the failure time at one-half the strength at liquid nitrogen temperature.

is defined as $t/t_{0.5}$ where $t_{0.5}$ is the delayed failure time at one half the strength at liquid nitrogen temperature. It should be emphasized that the abrasions studied covered only a small range of severe damage with correspondingly low strengths and that the curve was determined for soda-lime-silica glass tested at room temperature in distilled water.

2.5 The Theory of Charles and Hillig

Charles and Hillig[5] by refining the original model of Charles[4] developed a stress corrosion model that best satisfies the available experimental data. They considered an isotropic, brittle material as an elastic continuum which chemically reacts with its environment. Failure of the material under load was attributed to an alteration, by a corrosion reaction, of the geometries of pre-existing flaws or cracks on the surface. The model analyzed was an element of material under uniaxial stress and containing a semi-elliptical surface flaw. The equation developed for the velocity of a moving crack in a corrosive environment and having a crack tip stress σ was

$$v = v_o \exp - (- V^{*}\sigma + C\sigma^2 + \Gamma V_m/2\rho)/RT \tag{3}$$

where v_o represents the corrosion rate for a stress free surface and V^{*} is termed the activation volume. The term $C\sigma^2$ represents the combined effect of the disappearance of strain energy and a second order term in the expansion of activation free energy. The term $\Gamma V_m/2\rho$ represents the effect of curvature of the reaction

surface. Γ is the surface free energy of the glass-corrosion product interface. V_m is the molar volume of the glass and ρ is the radius of curvature of the crack tip. Charles and Hillig utilized the above velocity equation to derive a differential equation expressing the change of flaw contour with time. Three different changes in flaw geometry dependent on the level of applied stress are illustrated in Fig. 2. In Fig. 2a the glass is under no stress and the corrosion process attacks all surfaces uniformly. This rounds out the flaw tip and leads to a reduction in stress concentration and an increase in strength. This is what occurs, for example, on etching glass in hydrofluoric acid. When the applied stress is just insufficient to cause immediate fracture, it is assumed that corrosion takes place more rapidly in the highly stressed region near the crack tip. The crack lengthens and sharpens with time, which increases the stress concentration until eventually catastrophic failure occurs, Fig. 2c. At some intermediate applied stress the sharpening of the flaw by stress corrosion is balanced by the rounding out effect and the stress concentration of the flaw remains constant, Fig. 2b. This accounts for the existance of a fatigue limit in static fatigue.

By making various assumptions about flaw geometry and size, the following basic equations for static fatigue were derived:

$$S_L = \left[\frac{3\sigma_u \Gamma V_m}{8 V^* L} \right]^{\frac{1}{2}}$$

(4)
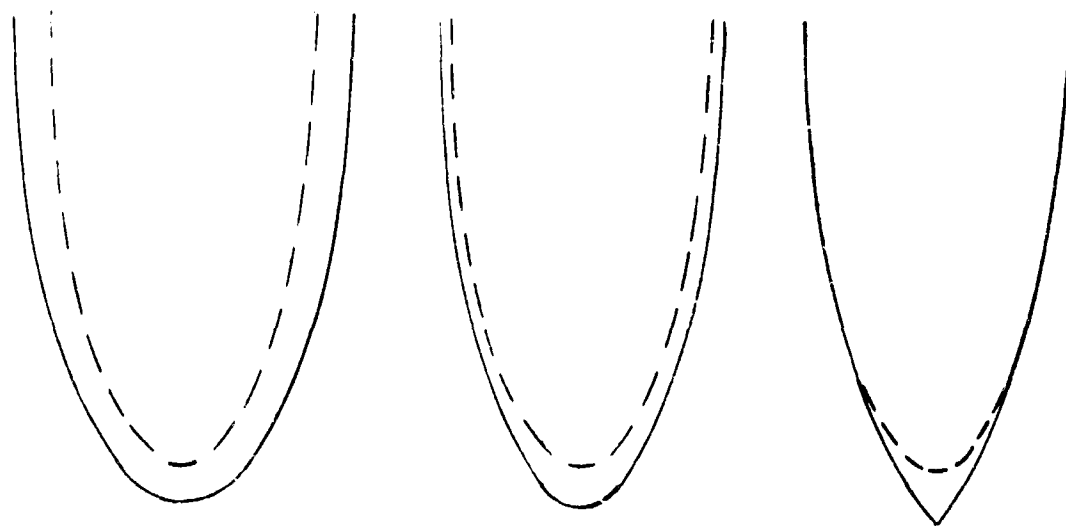
Figure 2. Hypothetical changes in flaw geometry due to corrosion or dissolution: (a) flaw rounding by corrosion; (b) flaw growth such that the rounding of the tip by stress corrosion balances the lengthening of the flaw; (c) flaw sharpening as a result of stress corrosion (after Charles and Hillig[5]).

S_L is the fatigue limit stress, the applied stress below which no failure of the specimen can occur. σ_u is the theoretical strength of the material. L is the initial depth of the flaw. The other terms are as previously defined.

$$\ln t/t_{0.5} = -\frac{V^*}{kT}\sigma_u\left[\frac{\sigma}{\sigma_N} - \frac{1}{2}\right] - f\,(\sigma/\sigma_N) \tag{5}$$

$t/t_{0.5}$ is defined as the reduced time where t is the time-to-failure at one-half the liquid nitrogen failure stress. σ/σ_N is defined as the reduced stress where σ is the failure stress and σ_N is the failure stress at liquid nitrogen temperatures. It is important to note that static fatigue is not observed at liquid nitrogen tem-peratures, therefore σ_N reflects the initial flaw size of a given sample without prior flaw growth. $f(\sigma/\sigma_N)$ is a slowly varying function which relates the short time behavior of the fatigue system to the time behavior of the system as it approaches the fatigue limit. Thus, this theory provides a basis for the broad understanding of the delayed failure process in terms of readily interpretable parameters and allows quantitative predictions to be made of the effect of temperature, corrosive environment, surface tension, etc.. By comparing the experimentally determined slope and fatigue limit of the universal fatigue curve of Mould and Southwick with the expectations of Eq. (4) and (5), Charles and Hillig obtained rea-sonable values for the parameters σ_u, V_m, V^* and Γ and the experi-mentally measured quantities L and S_L.

2.6 The Crack Velocity Measurements of Wiederhorn

Wiederhorn[9] used the double cantilever cleavage technique
to study the effect of water vapor on crack propagation in soda-
lime glass. He found the crack motion could be divided into three
regions. In Region I the crack propagation was due to the corrosive
attack of water vapor on the glass at the crack tip. The crack
velocity in Region II was believed to be limited by the rate of water
vapor transport to the crack tip. In Region III an unknown propaga-
tion mechanism occurred which was independent of water vapor con-
centration.

From the crack velocity equation of Charles and Hillig,[5]
Wiederhorn[9] derived a relation that represented the crack velocity
behavior of Regions I and II, however, his theory only partially
explained the effect of water vapor concentration on crack velocity
in Region II. The disagreement was thought to be due to the un-
certainty of the chemical reactions occurring at the crack tip
and the assumption of a constant boundary layer thickness at the
crack tip. No satisfactory explanation was found for crack propaga-
tion in Region III.

Recently Wiederhorn[10] showed that his data may be represented
by a velocity equation of the form

$$v = v_0 \exp - (E^* - b K_1)/RT \tag{6}$$

where K_1 is the stress concentration factor for the notched double
cantilever configuration and b, v_0, and E^* are experimental constants

determined by fitting the above equation to crack velocity measurements on a particular glass. Wiederhorn[9,10] tested various silicate glasses at relative humidities ranging from 0.017% to 100% and temperatures from 2° to 90° C. He found that while v_o was a strong function of relative humidity b was not. Using the relationship between stress intensity factor, applied stress and crack length, he integrated Eq. (6) and showed that the time to failure in a static fatigue test is

$$t = (2L_1/K_1^2 \, v_o \, \exp(-F*/RT)) \int_{K_1}^{K_{1C}} K \, \exp(-bK/RT)dK \qquad (7)$$

where L_1 is the initial crack length, K_1 is the initial stress concentration factor, K_{1C} is the critical stress concentration factor for failure in liquid nitrogen and R and T have their usual significance. From Eq. (7) he then derived that

$$K_1/K_{1C} = \sigma/\sigma_N = 0.5 - (2.3RT/bK_{1C})\log_{10}(t/t_{0.5}) \qquad (8)$$

where σ is the applied stress in a static fatigue test and σ_N is the failure stress at liquid nitrogen temperature. All other terms are as previously defined.

Equation (8) is the form of the universal fatigue curve. Since b and K_{1C} are independent of relative humidity, Eq. (8) predicts that a universal fatigue curve is independent of relative humidity. Therefore static fatigue data for a given chemical

composition and fixed temperature should lie along the same uni-
versal fatigue curve regardless of what relative humidity is chosen
for testing. The equation also predicts that the effect of increasing
temperature on a universal fatigue curve should be to increase the
slope in the negative sense.

Eq. (8) may also be rearranged to get

$$\sigma = (-2.3RT\sigma_N/bK_{IC})\log_{10}t + (0.5\sigma_N + 2.3RT\sigma_N/bK_{1C})\log_{10}t_{0.5} \qquad (9)$$

This is the form of static fatigue curves presented in the usual
way (failure stress versus log time to failure). Eq. (9) predicts
that static fatigue curves for a given chemical composition and
temperature but determined at different relative humidities are
parallel and are just shifted with respect to one another by an
amount determined by $\log t_{0.5}$.

2.7 Glass Fibers

The strengths of glass fibers are greater than any of the
commonly available materials of construction. Pristine E-glass
fibers exhibit average strengths of 5.2×10^5 psi in room environment
and 8.2×10^5 psi at liquid nitrogen temperatures.[18] It is thought
that the strength at liquid nitrogen temperatures represents the
theoretical strength of undamaged glass fibers. At liquid nitrogen
temperatures thermally activated corrosion processes are practically
inoperative. It is believed that in undamaged fibers fracture is
initiated by interstices in the atomic structure. The lower strengths

in room atmosphere are believed to result from static fatigue.

2.8 Static Fatigue of High Strength Glass Fibers

Static fatigue curves for E-glass fibers from various investigators are shown in Fig. 3. Both Otto[19] and Hollinger et al.[20] took their data at room temperature and 50% relative humidity. Schmitz and Metcalfe[21] obtained their data at 100% relative humidity and temperatures between 82° and 86°F. The curve and data points marked Hollinger, et al., was obtained by reading the data points from a plot in Reference 20 then taking the least squares line. The curve marked Otto is the line through his data as read off his graph by the present author. The curve and data points marked Schmitz and Metcalfe were read from Reference 21. From Fig. 3 it can be seen that the static fatigue curve of E-glass does vary somewhat from investigator to investigator. This could be due to differences in temperature, chemical composition, handling, or manufacturing processing. It is interesting to note that Schmitz and Metcalfe[21] did not observe a fatigue limit but instead a drop off in their data. The reason for this is unknown.

Pure fused silica is believed to be the strongest of the silicate glasses. Morly et al.[22] have obtained average strengths of 8.5×10^5 psi in room atmosphere with fibers of fused silica. In liquid nitrogen strengths increased to 2.0×10^6 psi. Proctor et al.[23] investigated static fatigue of fused silica at 30°C and 100% relative humidity. Figure 4 shows the line he determined through his data as read by the present author from a plot in Refer-
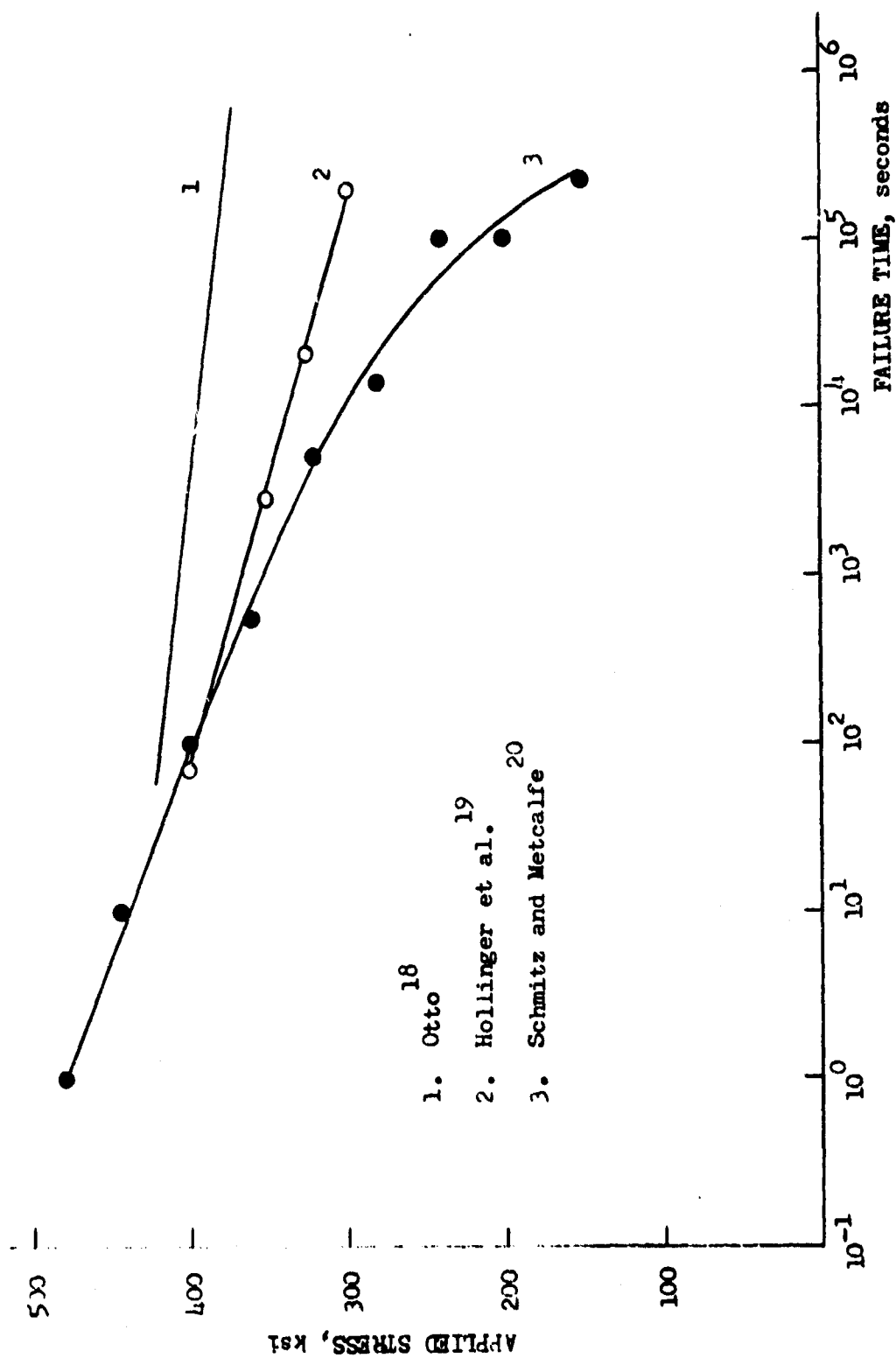
Figure 3. Static fatigue of high strength E-glass fibers

Figure 4. Static fatigue of fused silica fibers after Proctor et al.[23]
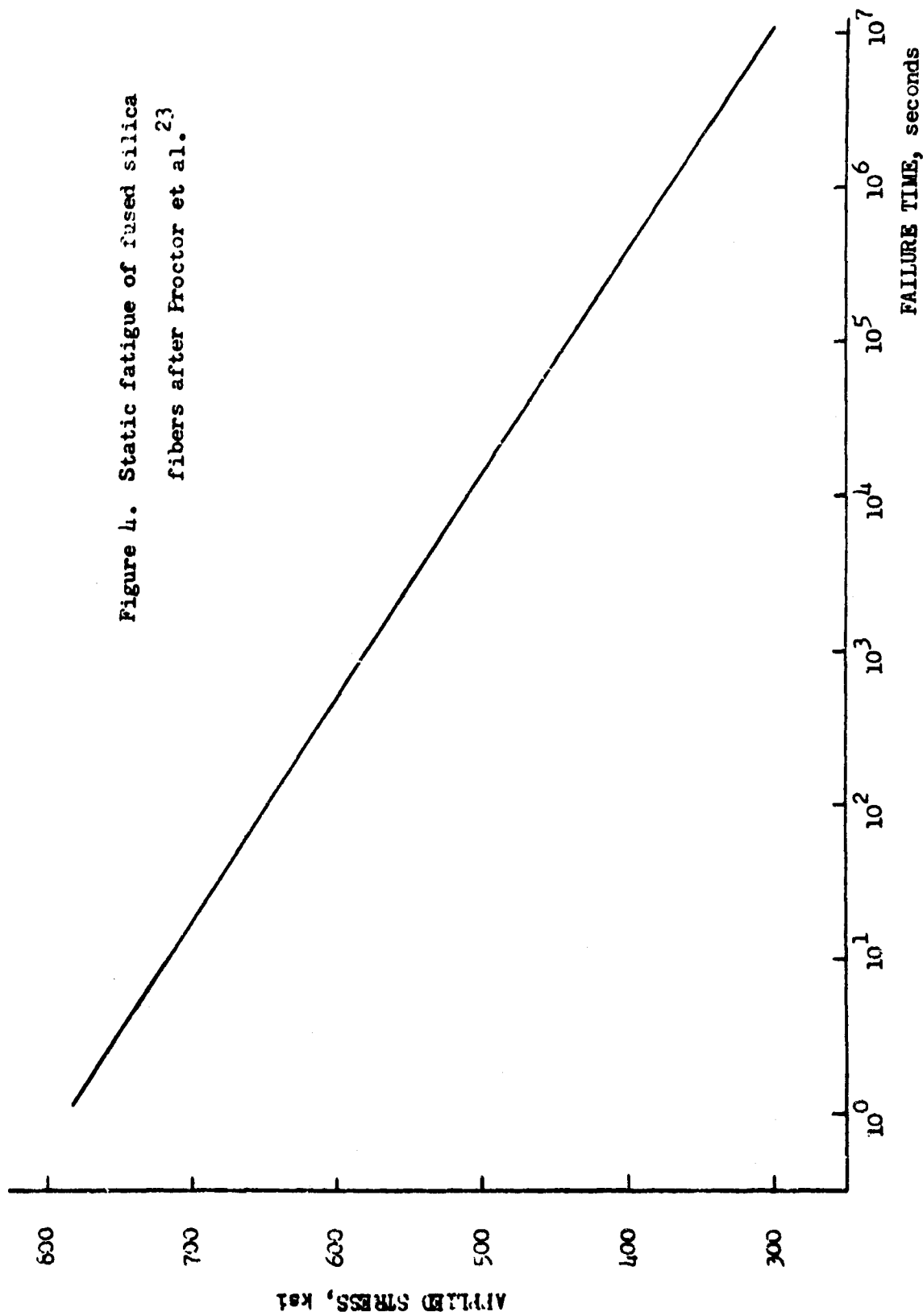
 once 23. The remarkably high strength of fused silica is evident

by comparison with E-glass Fig. 3.

3.0 PLAN OF WORK

After reviewing previous literature, it was proposed to experimentally determine the static fatigue curve (failure stress vs time to failure) of high strength, acid etched, soda-lime-silica glass rods at $74°F$ and relative humidities of 50% and 100%. These results will be compared to the universal fatigue curve of Mould and Southwick[15] and theoretical predictions of the stress corrosion theory of Charles and Hillig.[5] Using this stress corrosion theory, fundamental parameters describing stress corrosion will be determined. By making additional static tests at 100% relative humidity and different temperatures, an attempt will also be made to determine the apparent activation energy for stress corrosion.

In addition, the susceptibility to stress corrosion of fused quartz and borosilicate glass will be determined by measuring the dependence of strength on stressing rate. The results will be analyzed in the light of Weiderhorn's[9,10] crack velocity studies and Charles' theory[3] of dynamic fatigue. An effort will be made to correlate Wiederhorn's fundamental crack velocity data with the dynamic fatigue data of various silicate glasses.

4.0 PREPARATION OF ACID-ETCHED RODS

Kimble R-6 soda-lime-silica glass rods 3mm diameter were cut to 8 inch lengths. They were then annealed for one hour and furnace cooled. Initially rods were annealed at 450°C, later annealing was done at 500°C. Annealing reduces residual stresses,[8] promotes a more uniform glass network,[11] and reduces variability of results. The etching apparatus is shown in Fig. 5. A commercial stirrer running through a seven to one speed reducer turns the rod holder at approximately 90 rpm. Eleven rods may be placed in the plexiglass holder at one time. Rods are held at the ends to prevent them from touching each other during etching. Approximately .025 inch was etched off the diameter of each rod in a water solution of 15% hydrofluoric and 15% sulphuric acid. According to Proctor,[24] this is sufficient for maximum strength. During etching the holder was occasionally stopped and one rod, separate from the others, was rapidly removed, measured, and replaced as a check on sample diameters. After etching this rod was discarded. The ten other samples were rinsed in tap water and dried by dipping in acetone. Care was taken during handling so that the rods were never touched beyond $1\frac{1}{4}$ inches from either end. The inner span of $5\frac{1}{2}$ inches was then always available for testing.

Acid-etched rods $5\frac{1}{4}$ inches long were also required for experiments. These were made by cutting down previously annealed 8 inch lengths. Etching was done in a smaller plexiglass holder. Rods were held only at the bottom since their short length prevented them from touching each other during etching. Care was taken in
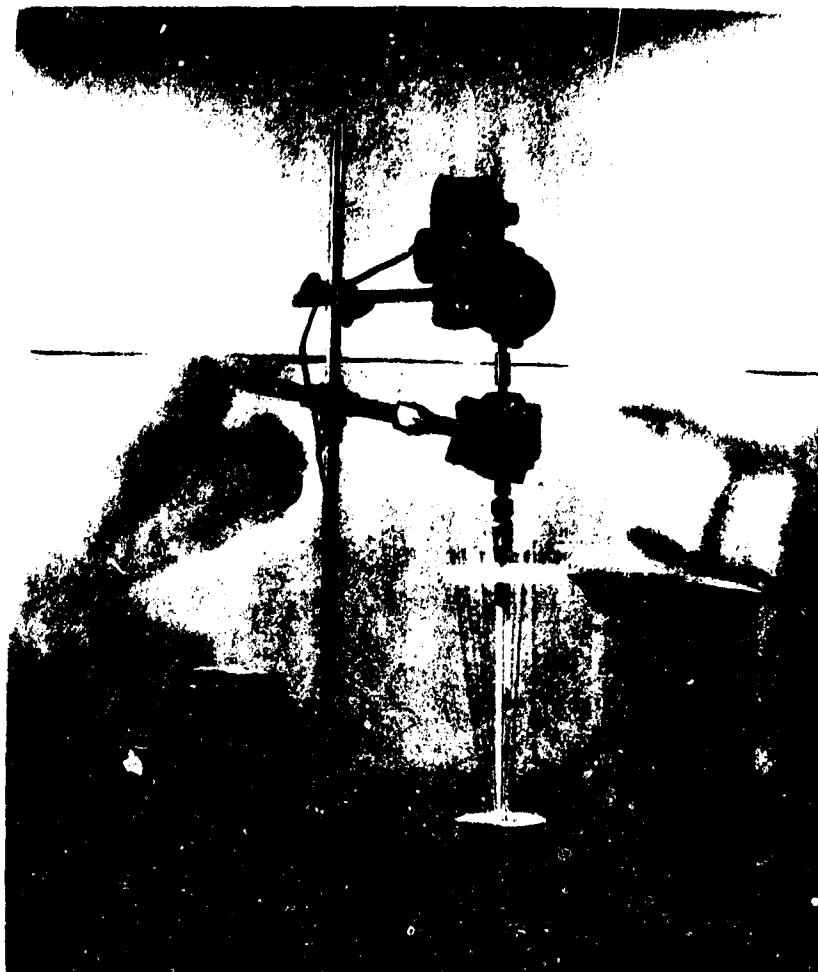
Figure 6. The etching apparatus.

handling so that these rods were never touched more than 3/4 inch in from either end. An inner span of 3 3/4 inches was always available for testing. After preparation acid-etched rods were stored in a dessicator (Section 9.1) or tested immediately.

5.0 PREPARATION OF ABRADED RODS

The abrasion apparatus, similar to that of Caporali[26], is shown schematically in Fig. 6. It was used to produce a controlled reproducible abrasion in the sample surface. In operation compressed air is regulated to 7 psi and fed to the grit supply and grit blast inlets. The motor is adjusted to rotate the glass rod at approximately 250 rpm. The compressed air is turned on for 5 seconds. Number 240 silicon carbide grit is blown through the blast nozzle against the sample and the result is shown in Fig. 7. Although the visible area of highest flaw density is relatively small, it should be noted that practically the entire length of the sample is exposed to abrasion during blasting. After blasting the samples were rinsed in distilled water to remove any clinging grit. They were then ready for ageing treatment (Section 8.3) or immediate testing.

A: Grit reservoir plug

B: Grit reservoir

C: Air inlet 7 psi

D: Solder fill

E: Blast funnel

F: Glass rod

G: Aluminum coupling

H: Electric motor 250 rpm

I: Waste outlet

J: Rubber plug

K: Air inlet 7 psi

L: Grit entry
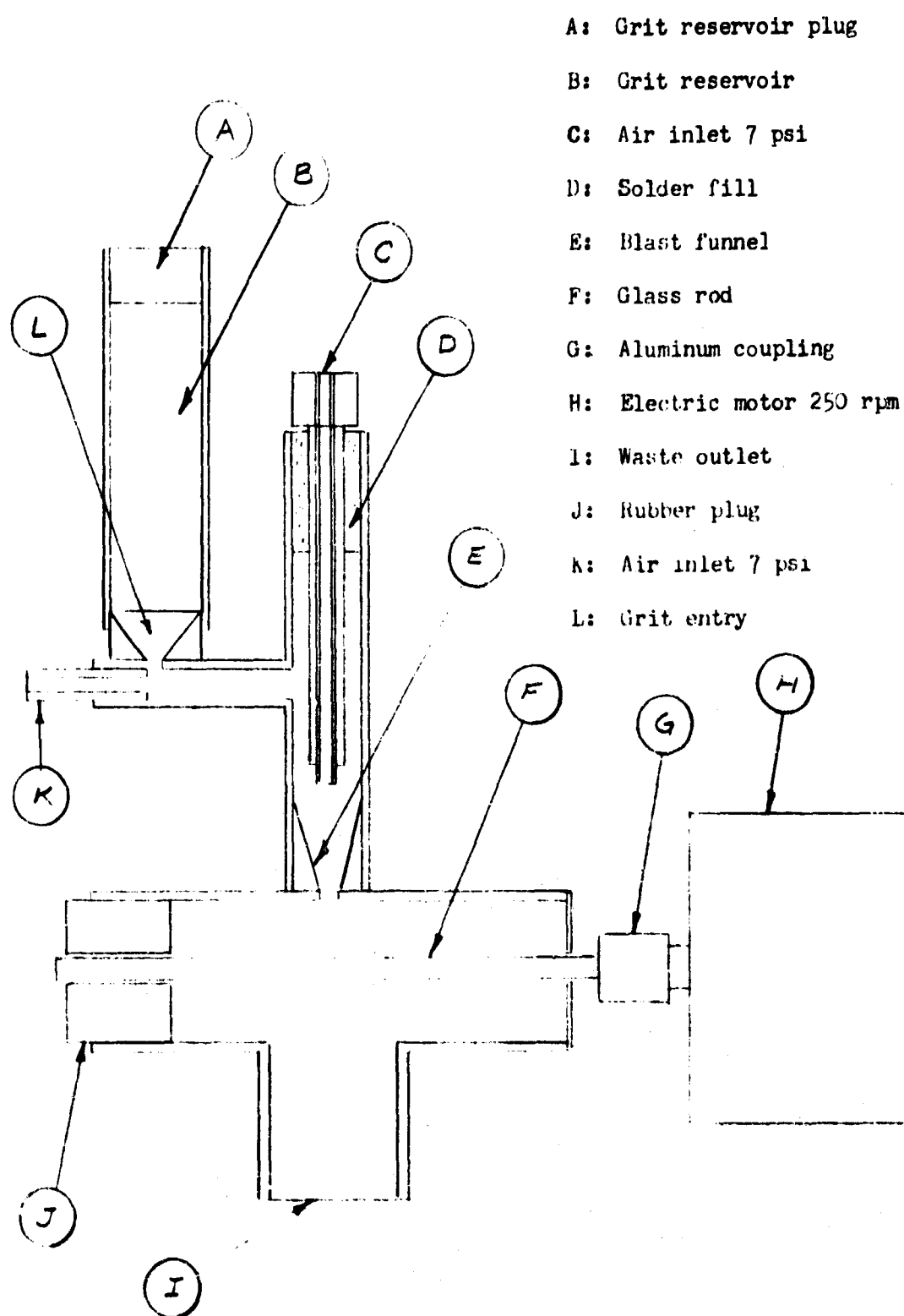
Figure 6. Abrader schematic

Figure 7. Abraded sample

6.0 DYNAMIC APPARATUS

The dynamic apparatus used by Ritter[6] to measure breaking strength in a dynamic test was mounted in an Instron universal testing machine. This is a four point bending apparatus with inner and outer spans of 0.813 and 2.808 inches respectively. The supports are ball bearings of 0.750 inch diameter. The inner rollers are fitted with brass sleeves having a peripheral radial groove with a diameter of .760 inch. This groove enables a specimen to sit stably on the center rollers while the outer rollers are brought into contact with it. Cross head speed on the Instron could be varied from .005 to 5 cm/min. The specimen is accessible during test so that it can be wetted if desired.

7.0 STATIC APPARATUS

7.1 The Buckling Instability in Four Point Bending

In investigating the fatigue behavior of pristine soda-lime-silica glass in four point bending, large deflections are imposed on the glass rods. These large deflections lead to non-linear relations between load and deflection. Therefore, the assumptions of simple beam theory are no longer applicable. These assumptions include that the reactions at the supports are vertical, and that the term $(dy/dx)^2$ is small compared to unity in the expression for curvature. Also, the effect of shifting of the point of tangency at the load and support points is not considered in simple beam theory. Therefore, for large deflections the complete non-linear differential equation governing beam deflection must be solved and corrections made for changes in geometry during loading as well. Recently this has been done by Vrooman and Ritter[25] using numerical techniques. Their solution shows that in a four point bending test with large deflections simple beam theory may result in a significant error in comparison with the numerically calculated stress. They also show that above a certain load a sample will buckle and pull through the outer span. The stress corresponding to the buckling load represents the maximum stress that can be measured. All the fracture stresses for acid-etched glass specimens where large deflections occurred were calculated using the numerical analysis of Vrooman and Ritter.

7.2 Testing Stations

Two types of testing stations were used to investigate static fatigue. These were basically similar in design and were termed types A and B. Dimensions of the A type testing station are such that four samples could be tested simultaneously inside the environmental chamber while only one sample could be tested using the type B station. Therefore, for static fatigue tests at the lower stress levels, where failure times are likely to be appreciable, the type A stations were used. The type B station was designed for tests at stress levels above the buckling stress of type A. It was anticipated that such tests would be required for high stress levels at 50% relative humidity.

7.21 Type A Static Fatigue Testing Stations

Fig. 8 is a schematic sketch of a type A static fatigue testing station. These stations were originally used by Ritter and Vrooman[27] and were modified for the present investigation. The load is applied to the glass rods in four point bending through a pivoted load arm. After a specimen fractures the load arm is caught by a rubber bumper to prevent shock loads in adjoining stations. The weights which are attached to the ends of the loading arms are commercially available kilogram sets having a tolerance of 1.0 grams per kilogram and are enamel coated to resist corrosive environments.

Failure times are recorded by eight electrical dig-

weight

loading arm

load carriage

microswitch

aluminum frame
and rubber pad

load
rollers

support rollers

sealed
bearing

microswitch

aluminum frame
and rubber pads
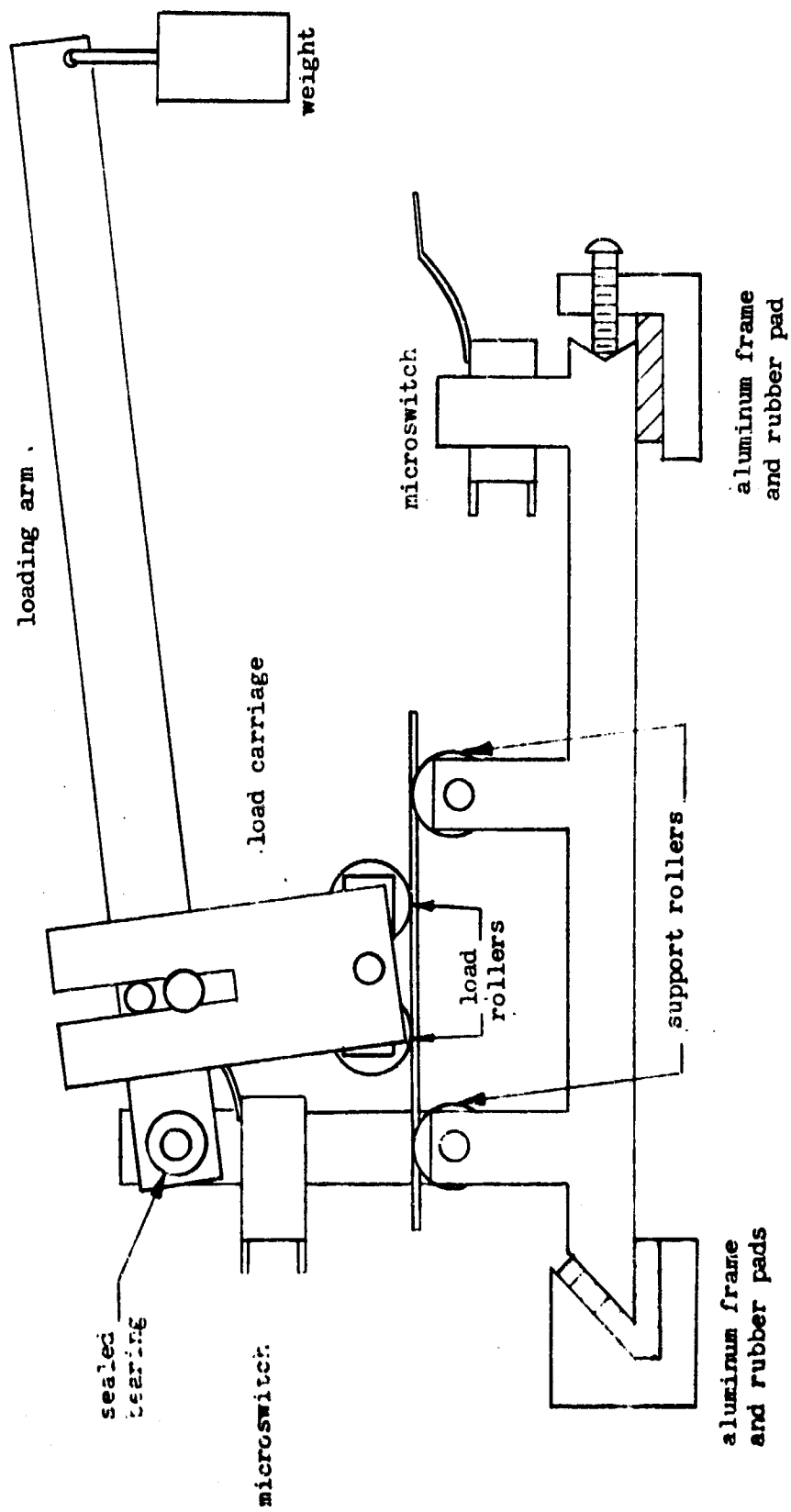
Figure 8. Schematic of type A static fatigue testing station

ital clocks mounted on a panel board which are turned on and off
by microswitches which sense the position of the loading arm during
specimen loading and after fracture. Two clocks are used for each
station. The first records the time in minutes and tenths of minutes
up to six digits. The second records the time in seconds and tenths
of seconds up to five digits. The electrical schematic is shown
in Fig. 9. Four parallel circuits of this type were used. All
materials in the fatigue apparatus are aluminum, brass, or stainless
steel to resist the corrosive atmosphere of water vapor used in
the fatigue tests.

The loading arm is 12 inches long, providing a nominal me-
chanical advantage of 6.857 to 1. The arm pivots in a .625 inch o.d.
sealed stainless steel bearing to reduce friction. The outer supports
are .750 diameter stainless steel rollers having a .125 inch radial
groove of .621 inch diameter. The grooves enable a glass rod to
rest stably in the center of the roller and provide accurate align-
ment of the specimen during testing. The load is applied at the
center of the $3\frac{1}{2}$ inch gage length between the outer rollers through
sealed stainless bearings of .625 inch diameter. The inner rollers
are 1.312 inches apart. Both the load and support rollers are pinned
to allow the glass rod to deflect with a minimum of friction at
the supports. In addition, the load bearings are attached to an
aluminum block which is pinned so that it can pivot in the loading
carriage. As the arm is lowered, two bearings adjust to a hori-
zontal position when they contact the glass rod and remain essentially

120V, 1PH
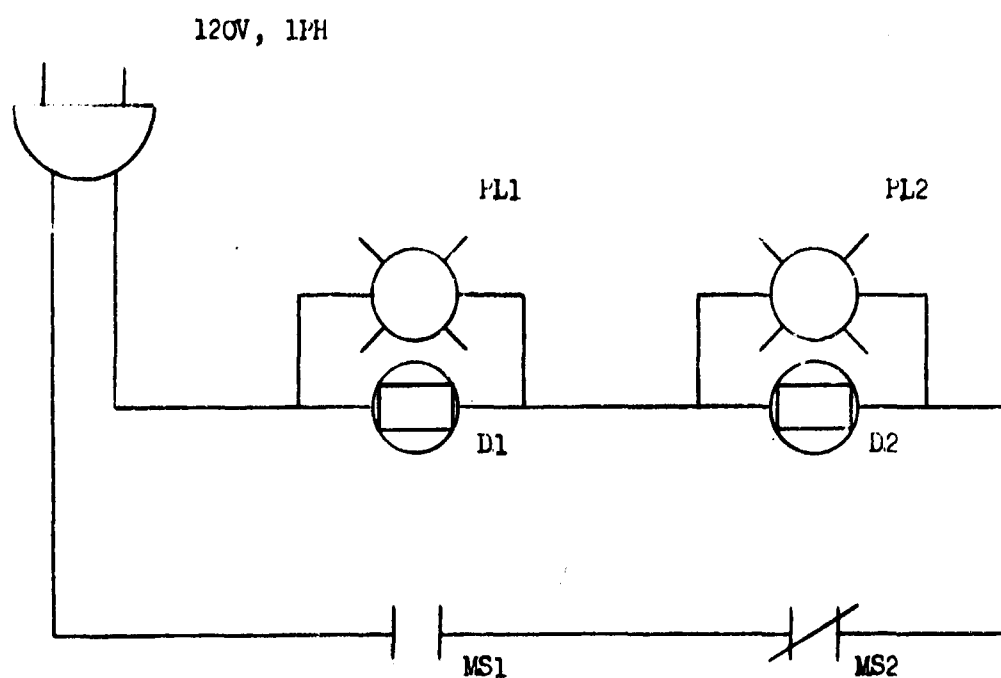
Figure 9. Static fatigue test station circuit

MS1 is the microswitch against the loading arm

and turns timers on during loading.

MS2 is the microswitch below the load arm to shut

timers off when sample fails.

D1, D2 are digital readout timers.

PL1, PL2 are pilot lights.

horizontal as the rod deflects. In this way four-point loading is
approximately maintained at all deflections, and a correction is
provided to compensate for any slight deviation of the arm from
horizontal in the fully loaded position. The load carriage which
is aligned perpendicular to the loading arm by a brass pin and a
brass carriage bolt, can be adjusted so that the loading arm is al-
ways horizontal when the samples are fully deflected, regardless
of the applied load.

The adjustment of the load carriages was first made
by adjusting the carriage on an extra station so that for a given
diameter glass rod and load, the loading arm was horizontal when
the glass rod was in the deflected position. The distance from
the top of the carriage to the top of the loading arm was then mea-
sured using the depth gage of a vernier caliper and the other fatigue
stations were adjusted to this dimension.

The nonlinear bending analysis of Vrooman and Ritter[25]
gives stresses as a function of rod diameter and the load parameter P,
equal to one half the load in pounds applied to the center rollers
of the bending apparatus. Although the nominal mechanical advan-
tage of the type A stations was 6.857 to 1, to compensate for the
weight of the loading arm and any slight variation in station di-
mensions the following calibration was done: The force exerted by
the unloaded arm was measured using a Toledo model 4031RA scale
having two pans and a dial reading from 0 - 2 lb. in 0.01 lb. in-
crements. The base of the station was clamped so that the load arm
was above one pan and the inner rollers pressed against the pan

through ground spacer blocks. Weights were added to the other
pan until the load arm was horizontal as measured by a bubble type
level. Weights used were commercial kilogram sets having a toler-
ance of 1.0 grams per kilogram. Then the scale reading was added
to the weight in the second pan and the weight of the spacers
was subtracted to give the weight of the unloaded arm. The mecha-
nical advantage was computed using the following formula:

$$A = \frac{\text{wt. in pan} + \text{scale reading} - \text{wt. of arm} - \text{wt. of spacers}}{\text{load}} \qquad (10)$$

Where A is the mechanical advantage and load is the weight hung
on at the end of the loading arm. Loads of 500, 1000 and 1500
grams were used and mechanical advantage was computed for each load.
This procedure was then repeated for the three remaining station.
The measured weights of the unloaded arms were then averaged.
The computed values of mechanical advantage for each station were
averaged and the average taken of these. The average arm weight
was 1.98 lbs. and the average mechanical advantage of all stations
was 6.85 in agreement with the nominal value of 6.857. Therefore,
for all stations the total force F in lbs. exerted on a specimen
by the center rollers was considered to be given by

$$F = 1.98 + 6.85 \times \text{LOAD (LB)} \qquad (11)$$

Since P is one half the total force, the relation between load hung
on the end of the loading arm in grams and P in lbs. is

$$\text{LOAD (Gm)} = \frac{(P-.99) \times 453.59}{\frac{1}{2} \times 6.85} \qquad (12)$$

For all static fatigue tests using type A stations, P was determined at a given stress level from a plot of the nonlinear analysis and the above equation was used to determine load. The average buckling stress of the type A station was 285,000 psi for the rod size range used. Therefore, static fatigue tests using the type A stations were not made at stresses above 270,000 psi.

To determine the minimum response time of the apparatus using the type A stations the following test was run. Loads of 3 kilograms were hung on the end of each load arm. This load is much greater than needed to fracture the glass rods and hence immediate failure results when the load arms are lowered. Acid-etched soda-lime-silica glass rods .098 inches in diameter were placed in the stations and when 74° F and 100% relative humidity was reached the arms were lowered and times to failure recorded. This procedure was repeated until 15 samples had been tested. The average time to failure was computed to be .003 minutes with recorded failure times ranging from .001 to .006 minutes.

7.22 Type B Static Fatigue Testing Station

Figure 10 is a photograph of the type B static fatigue testing station. The type B station was designed for use at stress levels above the buckling stress of type A and where static fatigue failure times were anticipated to be short. The type B static fatigue testing station is similar in design, construction, and operation

Figure 10. Type B static fatigue testing station

to the type A. Its principal features are reduced inner and outer spans, smaller rollers, and a longer loading arm.

The loading arm is 18 inches long providing a nominal mechanical advantage (geometrically calculated) of 16.74. The outer supports are .475 inch diameter stainless steel rollers and have a .125 inch radial groove of .375 diameter. The inner rollers, also of stainless steel, are .375 diameter. All rollers are pinned to reduce friction. The inner and outer spans are 2.150 and 0.750 inches respectively. A mercury switch attached to the load arm starts experiment timing instead of the normally open microswitch used on the type A. Timing is stopped when the sample fails and the load arm contacts a microswitch.

The force exerted on the center rollers by the unloaded arm of the type B station was determined by the same procedure as described for the type A except that a ground roller was placed between the inner rollers to decrease friction between the arm and the scale pan. The force exerted by the unloaded arm was found to be 5.99 lb. Previous experience with the type A stations in determining the mechanical advantage had shown good agreement between nomina (geometrically calculated) and measured values. Also, the force exerted by the center rollers of the type B station was far above the scale capacity of 30 lb. Therefore, the nominal value of 16.74 was used and for the type B static fatigue testing station the relationship between the weight in grams hung on the load arm and the load parameter P in lbs. from nonlinear bending analysis was

$$\text{LOAD(Gm)} = \frac{(P-3.00) \times 453.59}{\frac{1}{2} \times 16.74} \tag{13}$$

For all static fatigue tests using type B stations, P was determined from a plot of the nonlinear analysis and the above equation was used to determine load. The average buckling stress of the type B was 470,000 psi for the rod size range used. This was well above the highest anticipated testing stress for static fatigue.

To determine the minimum response time of the apparatus using the type B station the following test was run. A load of 4 kilograms was hung on the end of the load arm. This load is much greater than needed to fracture a sample and hence immediate failure results when the load arms are lowered. An acid-etched soda-lime-silica glass rod was placed in the station and when 74° F and 50% relative humidity was reached the load arm was lowered and the failure time recorded. This procedure was repeated until 10 samples had been tested. The average time to failure was computed to be .003 minutes with recorded failure times ranging from .001 to .005 minutes.

7.3 Environmental Chamber

Static fatigue tests were made inside a Develco Model MC08 temperature-humidity test chamber, Fig. 11. Chamber inside dimensions are 30 in. high x 24 in. wide x 22 3/4 in. deep. Wet and dry bulb temperatures are read on a Bristol Model 2T500FF-3B-3B-0i recorder controller from probes located inside the chamber. During testing 100% relative humidity was easily maintained at 74° F. However,

Figure 11. Environmental chamber

during the 50% relative humidity tests at 74°F the lowest relative
humidity obtainable varied between 50 and 58%. On hot, humid days
the refrigeration compressor would shut down automatically due to
overheating. This was finally cured by having a ⅓ hp fan with
two sirocco blades blow air through the condenser thereby increasing
cooling.

An aluminum rack was installed inside the chamber and leveled
for mounting of either type static fatigue testing station. Each
station was then mounted on rubber pads as shown in Fig. 8 as pro-
tection against external vibrations and vibrations caused by failure
of the glass rods in adjacent stations. The rack was slotted so
that sheets of plexiglass could be placed between the type A stations
to prevent fragments of broken glass rods from one station causing
failure in adjacent stations. An external crank was added and a
pulley system using nylon cords was built inside the chamber to
raise and lower the testing station loading arms. Fatigue tests
could be observed by turning on a light inside the chamber and
looking through the thermopane window in the chamber door.

8.0 EXPERIMENTAL PROCEDURE

8.1 Preliminary Investigations

8.11 Storage of Acid-Etched Rods

The effect of storage in vacuum and dry air was investigated to determine if acid-etched rods could be stored before testing without loss of strength. Acid-etched rods were produced as described in Section 5.1. A 10 inch diameter glass vacuum desiccator was obtained and two steel racks were made so that specimens could be placed horizontally in two layers inside the desiccator. A maximum of 35 rods could be stored in this manner and the desiccator was loaded with freshly etched samples several times. For dry air tests the desiccant used was either calcium chloride or a mixture of calcium chloride and Drierite (anhydrous calcium sulphate). For vacuum tests a mechanical pump was connected to the desiccator. A vacuum could be maintained at 0.08 Torr as read by a thermocouple sensor in the vacuum line. The desiccator was opened at intervals of from one to nineteen days. Groups of fourteen to thirty-one rods were removed and tested dynamically. A group of thirty-one samples were tested immediately after etching as a control.

8.12 Effect of Tygon Sleeves

It has been suggested in the literature that less variation is obtained in the breaking strength of glass rods when the rods are tested with short sleeves of tygon tubing at the ends

to prevent direct contact between the outer pair of rollers and the specimen. To determine if this was true, three groups of rods were tested using the dynamic apparatus described in Section 6.0. Acid-etched rods were freshly made in the usual way (Sect. 4.0), and fresh tygon tubing 1/8 i.d. x 3/16 l.d. was cut in one inch lengths. For the first series of seventeen rods the same two tygon sleeves were used throughout. These two sleeves had also been used to break two rods in practice runs. For the second series of 16 rods, new tygon sleeves were used for each rod. Throughout the testing care was taken in sliding the sleeves on the rods so that they did not come closer together than 2.1 inches which insured that the center span was not touched. A third group of nine rods was tested without sleeves as a control. Crosshead speed was 0.5 cm/min. Rods were tested dry in the laboratory atmosphere.

8.13 Surface Condition of Pyrex

Large variations in sample strength tend to mask other effects. Therefore, as preparation for later dynamic measurements the effect of surface condition on the variability in strength of Pyrex was studied. Mould and Southwick[15] have shown that in the case of soda-lime glass microscope slides, controlled abrasion reduced the variability in strength to standard deviations as low as 5 to 10% of the mean.

For the present study 3 mm Pyrex brand rod was cut into $5\frac{1}{2}$ inch lengths. The samples were then annealed at 565°C

for $\frac{1}{2}$ hour and furnace cooled. These samples were then used for tests with four surface conditions; grit blasted, acid etched, acid etched then grit blasted, and as-received. Etching was done by dipping samples into an etching solution of 15% hydrofluoric and 15% sulphuric acid in water for one minute. The samples were then removed and rinsed in tap water. The purpose of this light etch was to remove any gross mechanical damage in the as-received samples in the hope that there would be less variability in samples that were subsequently grit blasted. Grit blasting was done using the abrasion apparatus and method described in Section 5.0. After blasting the samples were rinsed in tap water. The as-received samples were also rinsed in tap water before testing. Tests were begun immediately after the samples were prepared. Dynamic tests were made in four point bending using the apparatus described in Section 6.0. Cross-head speed was 0.5 cm/min. Since abrasion leaves a small visible area of high flaw density around the center of the sample, Fig. 7, care was taken to position this region between the inner rollers during loading.

8.2 Static Fatigue

Static fatigue curves of high strength, acid-etched soda-lime-silica glass were experimentally determined at 74°F and 50% and 100% relative humidity. 100% relative humidity was easily maintained. However, during the 50% relative humidity tests, the actual relative humidity varied from 50% to 58%. In an attempt to obtain the apparent activation energy for static fatigue at 100% relative

humidity, additional data was taken at $100°F$ at stress levels of 200,000 and 210,000 psi, and at $50°F$ at a stress level of 200,000 psi.

Acid-etched rods were prepared (Sect. 4.0) and either tested immediately or stored before test in a closed desiccator. Rods were measured with a micrometer at both ends and the average taken as the true diameter. The required load parameter P was determined from plots of the nonlinear analysis for four point bending using the rod diameter and stress level desired. Separate plots were made for both type A and B testing stations. Fig. 12 is a sample plot of the solution for the type B testing station. Actual plots used were considerably larger. The load in grams to be hung on the test station loading arms was then determined from a computer tabulation of P versus load in grams from Eqn. (12) or (13) depending on the type testing station in use. The type A stations were used for all tests at 100% relative humidity, including the activation energy data. The type A stations were also used at 50% relative humidity for stress levels as high as 270 kpsi. It was anticipated that the type B station would be required at 50% relative humidity for tests at stress levels above 270,000 psi; however, data could not be taken at stresses above 270,000 psi since times to failure were less than the minimum measurable time to failure. Therefore, the type B station was also used at 50% relative humidity for stress levels from 230,000 to 270,000 psi.

Testing with the four type A stations was begun by establishing the desired temperature and humidity in the environmental chamber. This facilitates reestablishing these conditions after the chamber
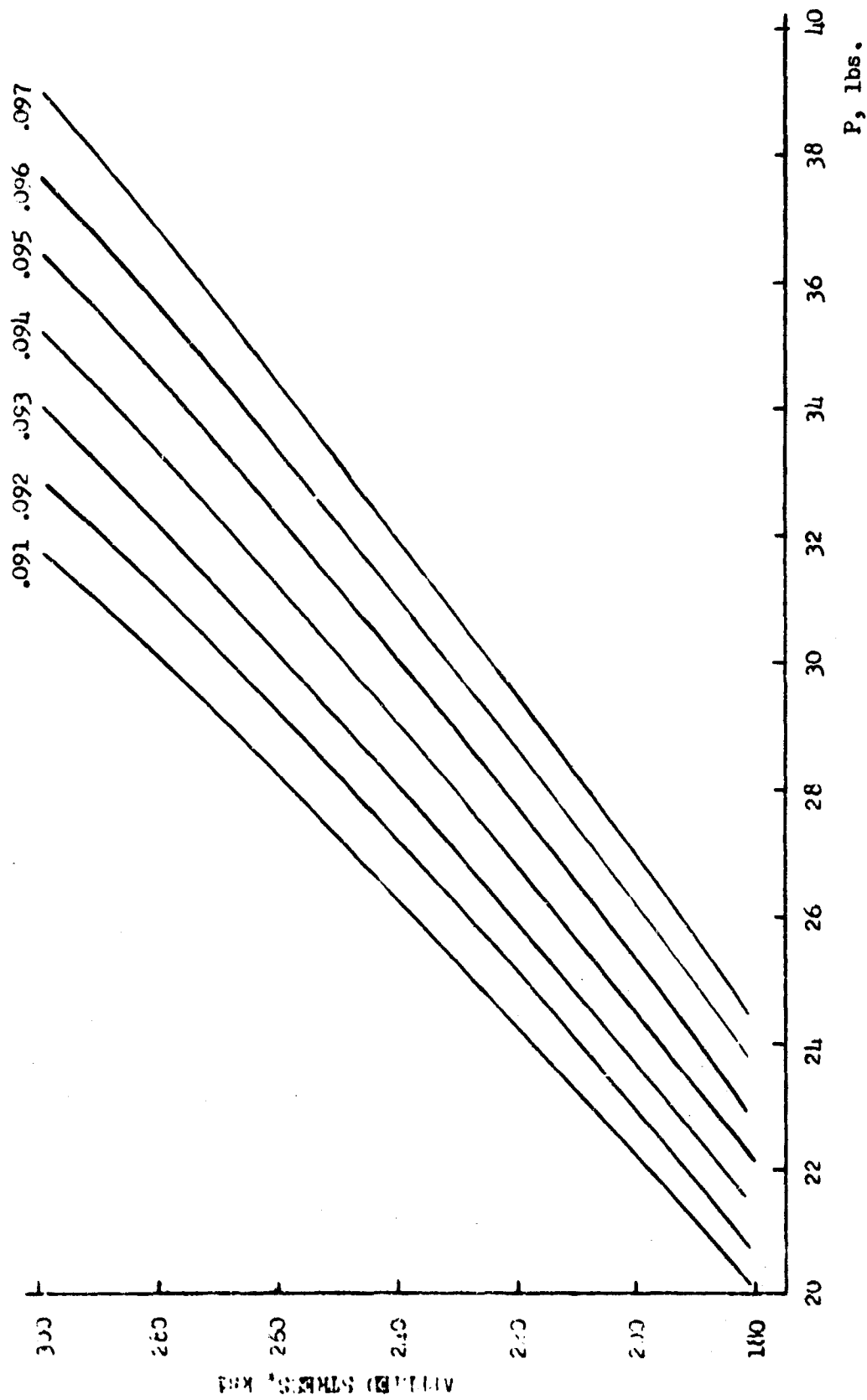
Figure 12. Calculated bending stress versus one-half the applied load for various specimen diameters for the type B static fatigue testing station

43

has been opened and the specimens placed in the bending ap[ ]ratus.
The external crank was then turned and locked to raise the loading
arms so that the etched rods could be placed in the fatigue stations.
The correct weights for each rod size and stress level were hung
on the station loading arms. The etched rods were placed on the
support rollers so that the etched, untouched portion overhung
the outer rollers on each end. Plexiglass shields were placed be-
tween the stations. The chamber was then closed and the desired
temperature and humidity reestablished. The timers were reset and
the crank was unlocked and rotated 3/4 turn to allow the load
rollers to lower on the glass rods. As each loading arm came within
$15°$ of horizontal, the individual microswitch on the arm started
the timers. After failure occurred at a station, the loading arm
dropped and tripped another microswitch which shut off the timers
for that station. The procedure for the type B station was similar
except that plexiglass shields were unnecessary and timers were
started by a mercury switch on the loading arm instead of a micro-
switch. Tests were generally terminated for samples that did not
fail after one day although in establishing the fatigue limit some
tests at low stresses were allowed to run for several days. Tests
to be used to determine activation energy were generally terminated
after one hour since the anticipated median failure time was within
that limit by two or three orders of magnitude.

8.3 Dynamic Fatigue

The susceptibility to stress corrosion of fused quartz and

pyrex (borosilicate) glass was determined by measuring the dependence of strength on stressing rate. The testing procedure for pyrex was as follows: Rods of 3mm Pyrex brand glass rods were cut to $5\frac{1}{2}$ inch lengths. The rods were annealed at $565°C$ for $\frac{1}{2}$ hour then furnace cooled. They were then abraded using the apparatus and procedure described in Section 5.0. After abrasion the samples were aged in distilled water for 5 hours. Mould[13] has shown that storage in distilled water is the most easily controlled and reproducible treatment for fresh abrasions before test. Groups of 20 samples were broken at each of 7 different crosshead speeds. These crosshead speeds were 0.005 0.01, 0.05, 0.1, 0.5, 1.0, and 2.0 cm/min. Samples were tested wet and at the lower crosshead speeds were periodically wetted with distilled water to insure that they remained wet during testing. A similar procedure was used to test 3mm fused quartz rods. However, fused quartz samples were not annealed due to the possibility of devitrification and were aged in distilled water 38 hours before testing.

9.0 RESULTS OF PRELIMINARY INVESTIGATIONS

9.1 Storage of Acid-Etched Rods

Results are summarized for both air and vacuum tests in
Table 1. The samples stored in vacuum for one day were evidently
mechanically damaged during storage as evidenced by the low strengths
and large variability. This damage probably occurred when the
vacuum line was accidentally pulled off the desiccator since an
oily grit was found in the vacuum connection of the desiccator.
The results of storage in the desiccator with air are shown graph-
ically in Fig. 13. Samples showed no discernable loss in strength
for storage times of up to 19 days. It was therefore concluded that
acid-etched samples could be stored in a closed desiccator before
test with no detrimental strength effects. Samples were generally
stored for less than one week with most being tested immediately
after etching.

9.2 Effect of Tygon Sleeves

Results for all three series of tests are summarized in Table 2.
The somewhat lower strengths recorded in series 1 when the same two
sleeves were used for all tests are probably the result of gross
mechanical damage. It is likely that the sleeves became impregnated
with broken glass or corrosion products from the surface of the rods.
Strengths recorded in the second and third series are comparable
and within the range of the desiccator storage experiments which
were conducted without tygon sleeves. Also, the second and third

TABLE 1

Effect of Storage on Strength of Acid-Etched, Soda-Lime-Silica Glass Rods

Storage in Dry Air

Days stored	No. samples tested	Average failure stress (psi)	Standard deviation (psi)	Coefficient of variation (%)	95% Confidence interval (psi)
0	31	310324	105777	34.1	271370 to 348948
1	18	345178	47793	13.8	319716 to 348958
3	14	291162	78997	27.1	245559 to 336766
7	15	305819	85523	27.9	258453 to 353185
19	20	334255	62284	18.6	305109 to 363409

Storage in Vacuum

Days stored	No. samples tested	Average failure stress (psi)	Standard deviation (psi)	Coefficient of variation (%)	95% Confidence interval (psi)
1	31	82249	80779	98.2	52622 to 111875
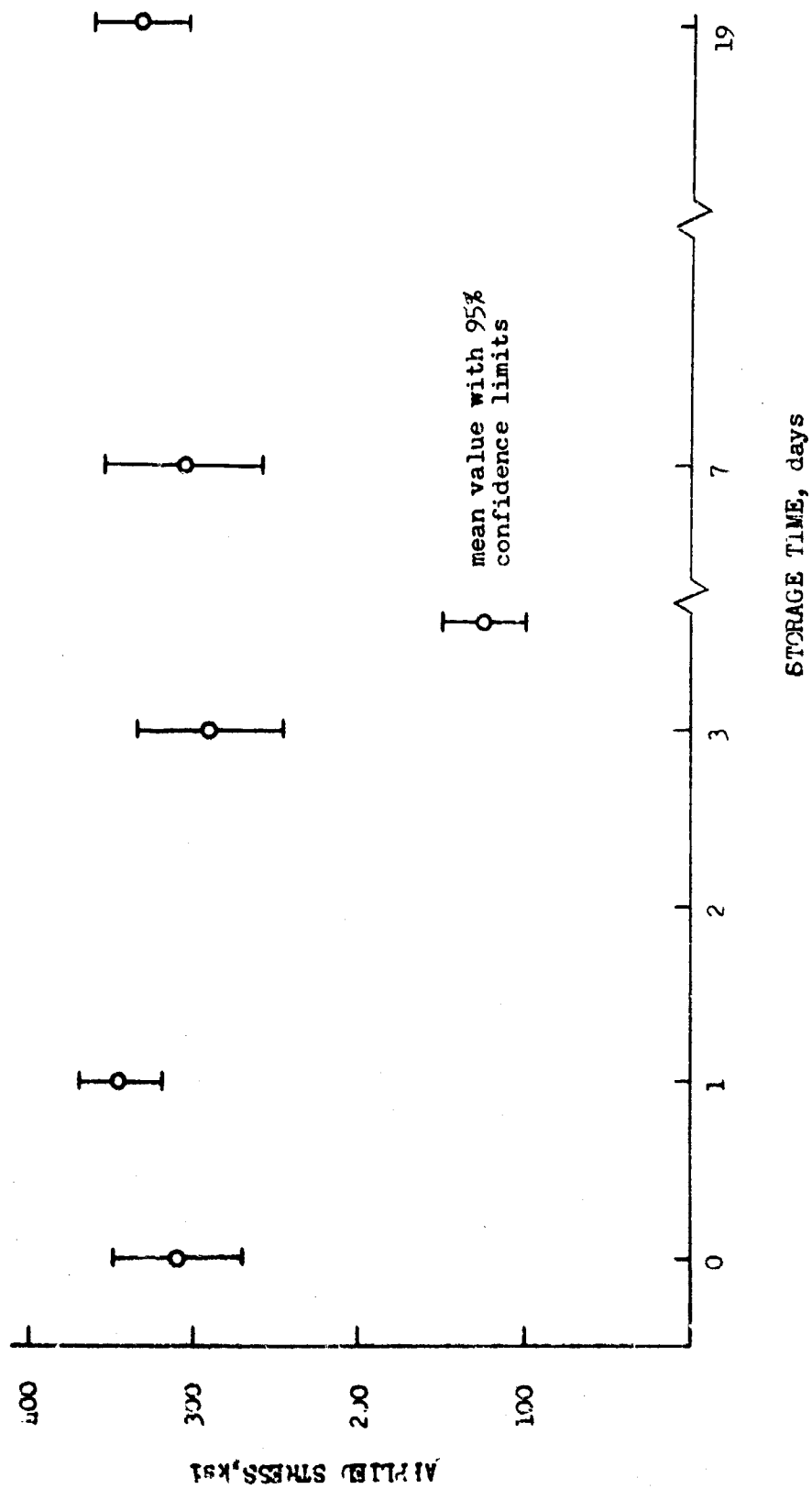
Figure 13. Effect of storage in dry air on strength

48

TABLE 2

Effect of Tygon Sleeves on Strength of Acid-Etched, Soda-Lime-Silica Glass Rods

Series 1 - Same sleeves used throughout

17 Samples

Mean (psi)	254536
Standard deviation (psi)	72805
Coefficient of variation (%)	28.5
95% Confidence interval (psi)	217401 to 292270

Series 2 - New sleeves each test

16 Samples

Mean (psi)	315036
Standard deviation (psi)	86952
Coefficient of variation (%)	27.6
95% Confidence interval (psi)	268712 to 361359

Series 3 - Without sleeves

9 Samples

Mean (psi)	282749
Standard deviation (psi)	66440
Coefficient of variation (%)	23.5
95% Confidence interval (psi)	231678 to 333820

series show similar variation in strength regardless of whether
the samples were tested with fresh sleeves or without sleeves.
Therefore, it was concluded that there was no advantage in using
tygon sleeves on the acid-etched samples.

9.3 Surface Condition of Pyrex

Results for all four surface conditions are summarized in
Table 3 and graphically in Fig. 14. The effect of abrasion was to
greatly reduce the variability of breaking strength since there
was no significant difference between the as-received abraded and
the acid-etched abraded samples. As-received samples, therefore,
were abraded in all subsequent dynamic testing. The large varia-
bility in breaking strength shown by the lightly acid-etched samples
and to a lesser extent by the as-received samples is a reflection
of the large distribution of flaw sizes expected to be found on
the surface of these glasses.

TABLE 3

Surface Condition and Strength of Pyrex

Series 1 - Acid etched

10 Samples

Mean (psi)	62669
Standard deviation (psi)	36805
Coefficient of variation (%)	58.7
95% Confidence interval	36342 to 88996

Series 2 - Acid etched and abraded

10 Samples

Mean (psi)	13605
Standard deviation (psi)	851
Coefficient of variation (%)	6.2
95% Confidence interval	12996 to 14214

Series 3 - Abraded

9 Samples

Mean (psi)	12887
Standard deviation (psi)	534
Coefficient of variation (%)	4.1
95% Confidence interval	12476 to 13297

TABLE 3 (continued)

Series 4 - As recieved

10 Samples

Mean (psi)	16054
Standard deviation	6338
Coefficient of variation (%)	39.4
95% Confidence interval (psi)	11520 to 20587
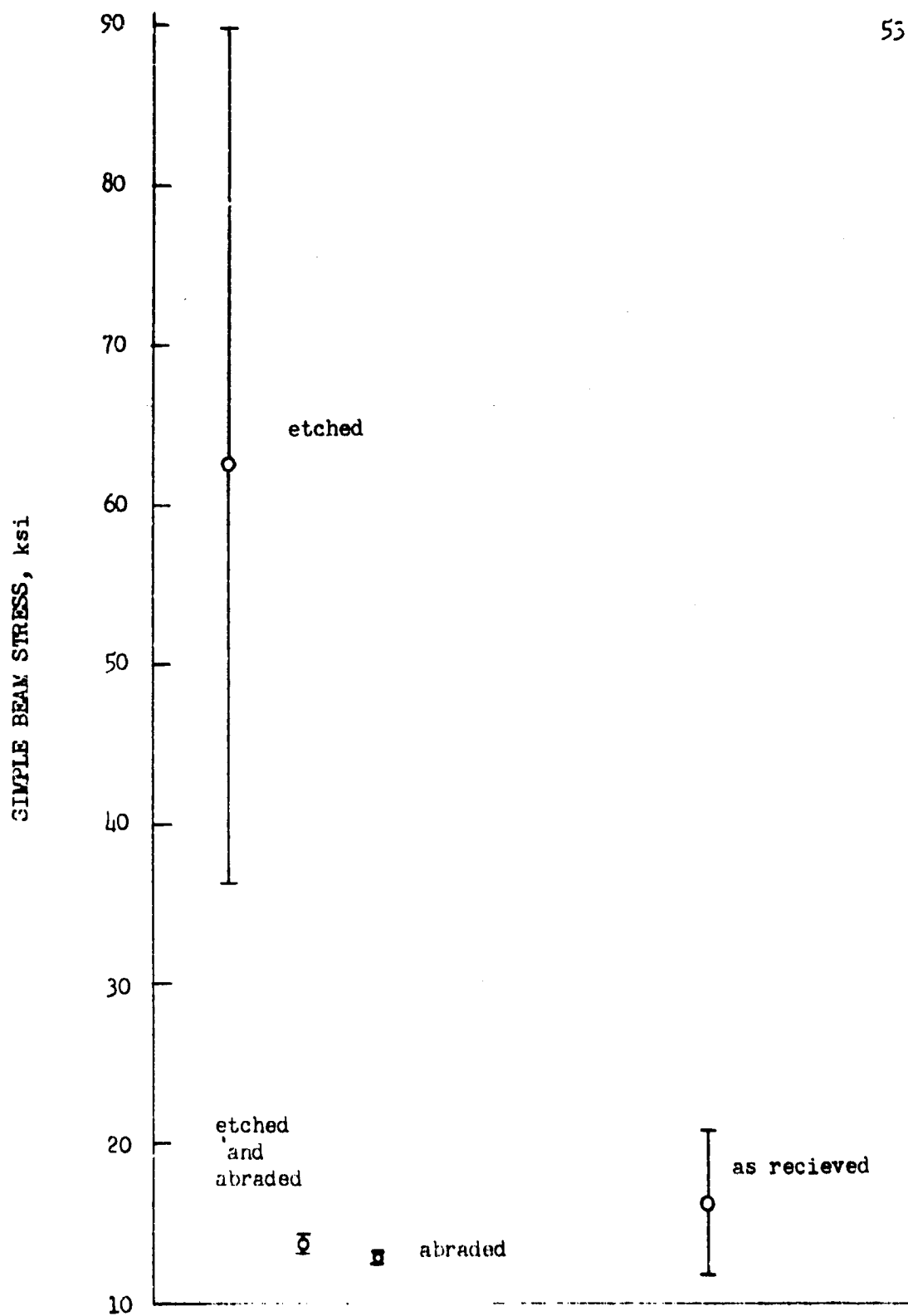
Figure 14. Surface condition and strength of pyrex

10.0 STATIC FATIGUE

10.1 Static Fatigue Data

Results of static fatigue tests of acid-etched, soda-lime-silica glass rods at $74°$ F are summarized in Tables 4 and 5 for 100% and 50% relative humidity respectively. Stresses and failure times are plotted in Fig. 15 and representative least squares lines are shown for both 100% and 50% relative humidity. Data points at 230,000 psi 100% relative humidity, and 270,000 psi 50% relative humidity, were used in fitting the lines although it should be noted that the corresponding failure times were approximately the minimum response time determined for the apparatus. The slope of the least squares line for 100% relative humidity is 14,619 psi/log decade and the intercept is 190,260 psi with a correlation -.992. The slope of the least squares line for 50% relative humidity is 14,419 psi/log decade and the intercept is 223,005 psi with a correlation of -.954. The static fatigue limit stresses, given in Tables 4 and 5, are 150,000 and 160,000 psi for 100% and 50% relative humidity respectively and are indicated in Fig. 15 by arrows in the appropriate data points.

Median times to failure determined for acid-etched, soda-lime-silica glass rods at 100% relative humidity for various temperatures and stress levels are shown in Table 6. It was hoped that these median times to failure could be used to compute the apparent activation energy for static fatigue, however, the data is too inconsistent to allow this calculation. For example, for

TABLE 4

Static Fatigue of Acid-Etched, Soda-Lime-Silica Glass at 74° F 100% Relative Humidity

No. of Samples Failing Within Indicated Time Decades -- Time in Minutes

Stress KSI	$<3 \times 10^{-3}$	10^{-2}	$\leq 10^{-1}$	10	10^1	10^2	10^3	10^4	10^5	No. Tested	Median Time
270	13	0	0	0	0	0	0	0	0	13	.0016*
250	47	13	0	2	0	0	0	0	0	62	.0016*
230	49	21	9	5	7	2	4	0	0	97	.0025
210	13	8	5	8	9	6	1	0	0	50	.0405
200	5	8	10	12	16	4	1	1[a]	0	57	.2141
180	9	12	1	5	8	11	6	9[b]	0	61	2.5500
170	2	2	0	4	15	11	7	16[a]	3[c]	60	40.7766
160	0	0	0	0	0	1	1	1[a]	0	3	
150	0	1	0	0	0	0	2	15[a]	4[a]	22	Fatigue Limit

*: Time less than minimum accurate timing for apparatus

a: Tests terminated samples survived

b: 2 samples failed 7 survived when tests were terminated

c: 1 sample failed 2 survived when tests were terminated

TABLE 5

Static Fatigue of Acid-Etched, Soda-Lime-Silica Glass at $74°F$ 50% Relative Humidity

No. of Samples Failing Within Indicated Time Decades — Time in Minutes

Stress KPSI	$<3 \times 10^{-3}$	10^{-2}	10^{-1}	10^{0}	10^{1}	10^{2}	10^{3}	10^{4}	No. Tested	Median Time
272	11	3	1	1	2	1	0	0	19	.0025
255	8	39	13	11	10[a]	4	4	6[b]	95	.0141
230	12	0	8	2	5	3	4	7[b]	50	.0437
215	1	2	4	8	11	9	3	2[b]	40	2.6995
200	0	3	2	6	9	6	10	13[b]	49	82.3466
180	0	0	0	1	0	0	0	6[c]	7	
170	0	0	0	0	0	1	0	4[d]	5	
160	0	0	1	0	0	0	0	14[b]	15	Fatigue Limit

a: 1 sample had test terminated

b: Tests terminated samples survived

c: 2 samples failed 4 survived when tests were terminated

d: 2 samples failed 2 survived when tests were terminated

56

Figure 15. Static fatigue of acid-etched, soda-lime-silica glass at 74°F

o 50% relative humidity
• 100% relative humidity
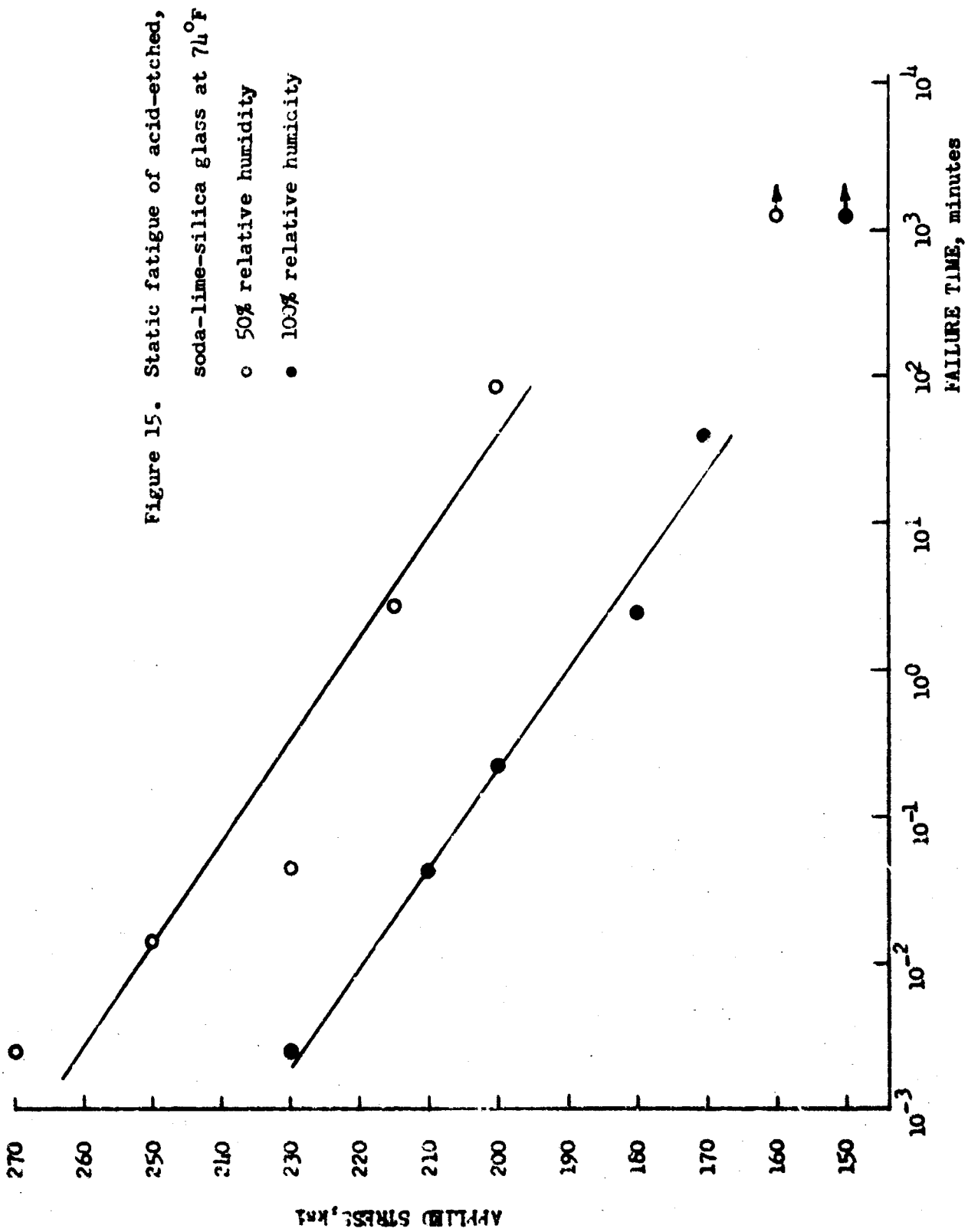
TABLE 6

Median Failure Times for Acid-Etched, Soda-Lime-Silica Glass

at 100% R. H. and Various Temperatures and Stress Levels

Temperature (°F)	Stress (kpsi)	Median failure time (min)	No. samples tested
100	210	.1066	31
74	210	.0400	from Fig. 15
100	200	.0084	40
74	200	.2040	from Fig. 15
50	200	.0075	60

Stress level 200,000 psi the time failure at $50°$ F and $100°$ is less than the time to failure at $74°$ F. This could be due to variability in the data and not taking large enough differences in temperature.

10.2 Comparison of Static Fatigue Data with the Universal Fatigue Curve of Mould and Southwick

Static fatigue results of high strength acid-etched, soda-lime-silica glass rods at $74°$ F and 100% relative humidity, Fig. 15, may be normalized in the reduced units of the universal fatigue curve of Mould and Southwick.[15] The reduced stress is defined as σ/σ_N, the failure stress divided by the failure stress at liquid nitrogen temperature. The value of σ_N for acid-etched, soda-lime-silica glass has been determined by Ritter[28] to be 4.705×10^5 psi. The reduced time is defined as log $(t/t_{0.5})$, where t is the failure time and $t_{0.5}$ is the failure time at one-half the liquid nitrogen stress. From Fig. 15, $t_{0.5}$ is found to be 8.92×10^{-4} min. at 235,250 psi. The effect of dividing t by $t_{0.5}$ is to shift the reduced fatigue curve so that log $(t/t_{0.5})$ is equal to 0.0 for σ/σ_N equal to 0.5. The slope of the reduced curve, shown in Fig. 16 is -.031. The universal fatigue curve obtained by Mould and Southwick for soda-lime-silica glass tested at room temperature in distilled water and having a variety of surface abrasions is shown dotted for comparison. The slope of the universal fatigue curve is -.078 which is about $2\frac{1}{2}$ times as great as the slope of the static fatigue data for acid-etched, glass rods. This large difference in slope
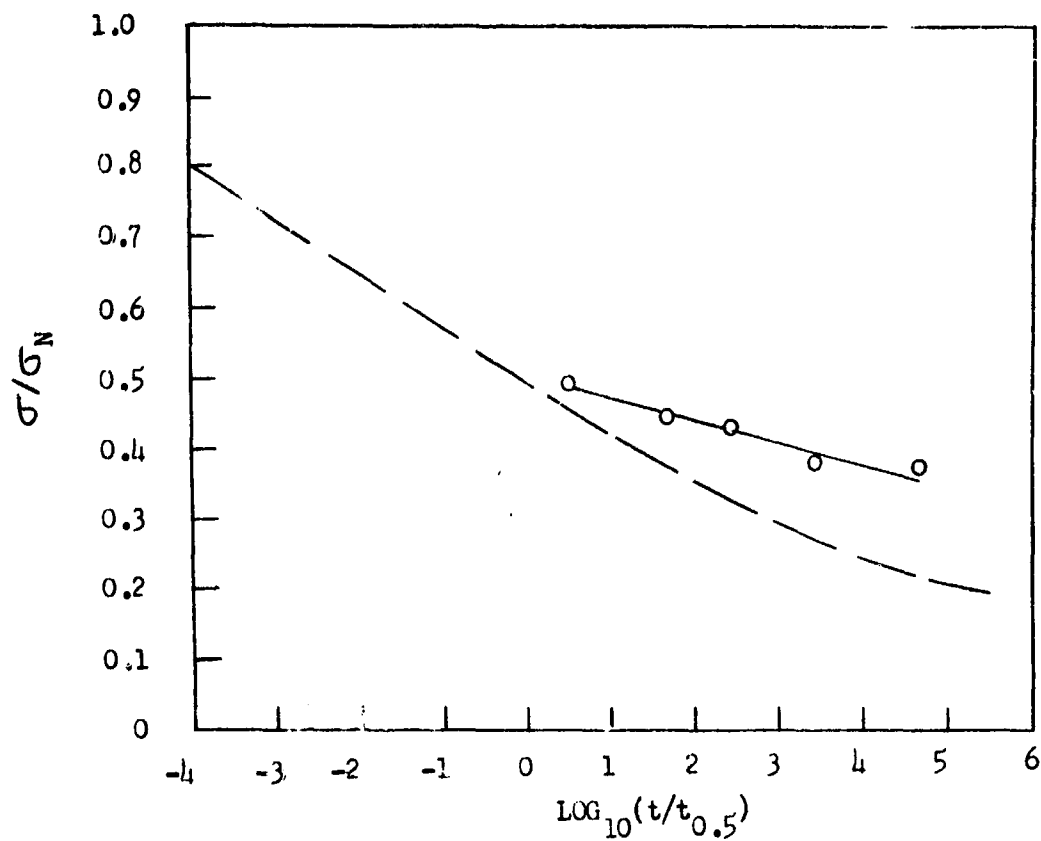
Figure 16. Static fatigue of acid-etched, soda-lime-silica glass at 74°F and 100% relative humidity plotted in units of reduced stress and time. Dotted curve represents universal fatigue curve of Mould and Southwick[15] obtained for abraded soda-lime-silica glass.

indicates that the universal fatigue curve does not apply to the static fatigue behavior of high strength, acid-etched, soda-lime-silica glass.

10.3 Comparison of Static Fatigue Data with the Theory of Charles and Hillig

The static fatigue theory which best describes the present experimental data is that of Charles and Hillig.[5] The expression for the slope of the line passing through the reduced static fatigue data given by Charles and Hillig is:

$$\frac{d \ln t/t_{0.5}}{d(\sigma/\sigma_N)} = -\frac{V^* \sigma_u}{RT} \tag{14}$$

All terms are as defined in Section 2.5. The activation volume for stress corrosion at 100% relative humidity may be calculated from the above equation. By choosing the value of σ_u to be 2×10^6 psi, and using the temperature of $74°$ F and the slope of -74.2 from the static fatigue date at 100% relative humidity the activation volume, V^*, is found to 13.2 cm^3/mole. The experimental fatigue limit stress, S_L is 1.5×10^5 psi (from Table 1) and the molar volume V_M is assumed to be 20 cm^3.[5] Using the above values of σ_u and V^* in Eqn. 4, Γ/L can then be calculated to be 1.355×10^9 ergs/cm^3. Using the Orowan criteria for failure[14] the crack depth, L, can be calculated to be 6.25×10^{-7} cm. Using this value of the crack depth, Γ is calculated to be 846 ergs/cm^2. The typical value of

the activation volume, V^*, for alkali metal ion diffusion in silicate glasses was reported by Charles and Hillig[5] to be $4.9 \text{ cm}^3/\text{mole}$. They calculated V^* to be 1 cm^3 for abraded soda-lime-silica glass using the slope of the universal static fatigue curve of Mould and Southwick.[15] Then using the data for a point on the universal fatigue curve near the fatigue limit, they calculated Γ to be approximately 500 ergs/cm^2. It should be noted that Γ is dependent on the values which are chosen for σ_N, the strength at liquid nitrogen temperatures, σ_u, the ultimate strength of the material, and L, the crack depth. There could be as much as an order of magnitude error in the choice of the crack depth, and σ_u and σ_N^- could vary by a factor of two. Therefore, the value of Γ could vary considerably depending on the choice of the above parameters.

11.0 DYNAMIC FATIGUE RESULTS AND THEORY OF CHARLES

The experimental data from dynamic fatigue tests of fused quartz and abraded pyrex are summarized in Tables 7 and 8. Figures 17 and 18 are log-log plots of these results. The straight line shown in each of these figures was calculated by the method of least squares with the slope as indicated. The correlation coefficient was .708 for fused quartz and .954 for pyrex. As discussed in Sect. 2.3 Charles[3] derived that under dynamic loading the breaking strength of glass should vary with the rate of stress application as follows:

$$\sigma_{af} = K \beta^{1/n+1} \tag{2}$$

where σ_{af} = macroscopic applied stress at which failure occurs, β = rate of stress application, n = exponent in Charles' assumed crack velocity equation and K = constant. Assuming simple beam theory the stressing rate is proportional to the loading rate at the load points. Therefore, from Fig. 17 the value of "n" for abraded fused quartz is 37.8 and from Fig. 18 the value of "n" for abraded pyrex is 27.4.

TABLE 7

Dynamic Fatigue of Abraded Fused Quartz

Loading rate at load points (cm/min)	Average failure stress (psi)	Standard deviation (psi)	Coefficient of variation (%)	95% Confidence interval (psi)
0.005	7459	1129	15.1	6930 to 7987
0.01	7913	1542	19.4	7191 to 8635
0.05	6379	1389	16.5	7728 to 9029
0.10	7097	1747	22.1	7079 to 8715
0.50	8103	1713	21.1	7301 to 8905
1.00	9716	2010	20.7	8775 to 10657
2.00	8468	1827	21.5	7613 to 9324

TABLE 8

Dynamic Fatigue of Abraded Pyrex

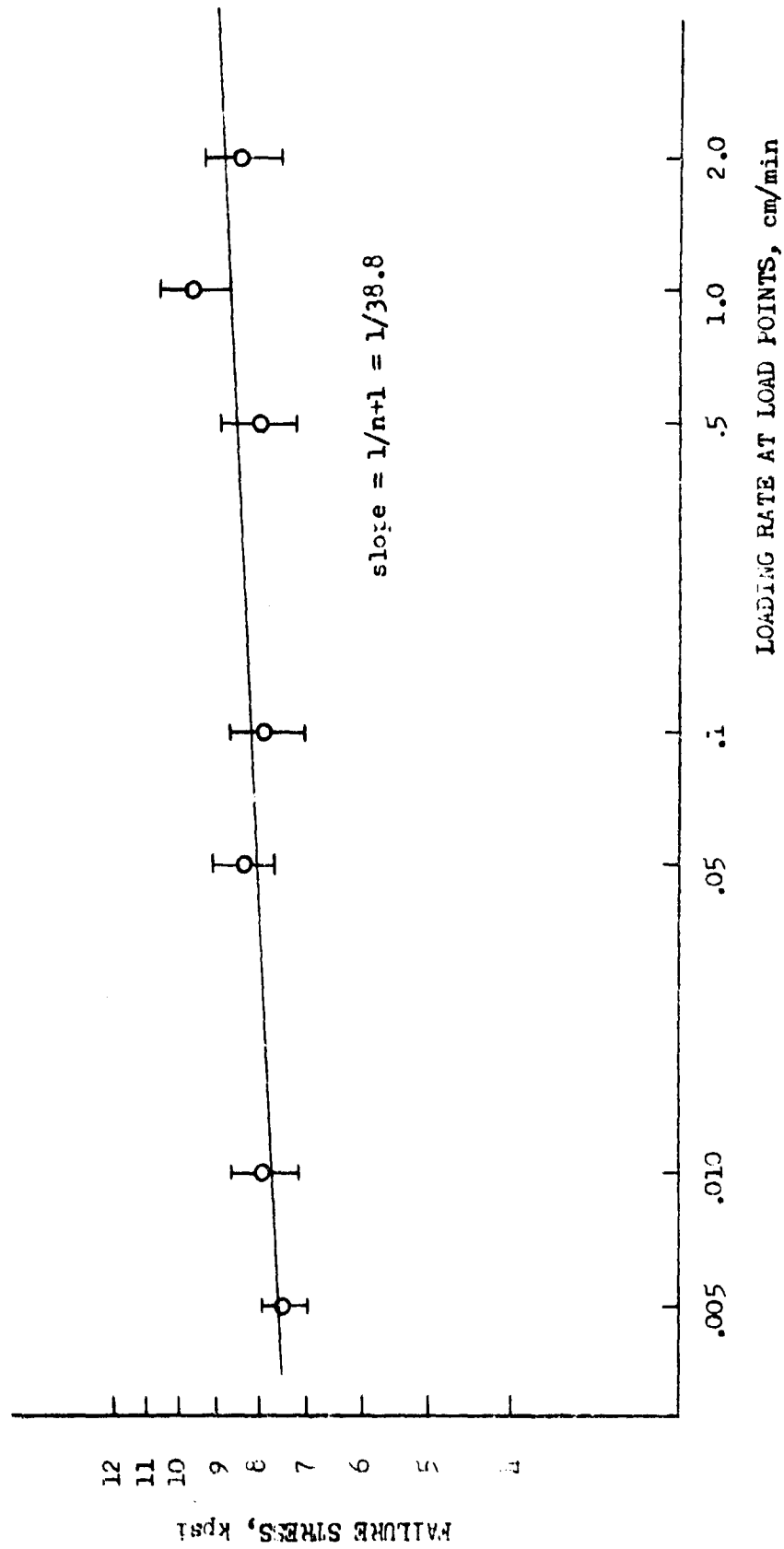| Loading rate at load points (cm/min)	Average failure stress (psi)	Standard deviation (psi)	Coefficient of variation (%)	95% Confidence interval (psi)
0.005	10720	853	7.9	10321 to 11120
0.01	10765	1026	9.5	10284 to 11245
0.05	11919	738	6.2	11573 to 12265
0.10	11794	1271	10.7	11200 to 12389
0.50	12476	1804	14.4	11631 to 13320
1.00	12370	896	7.2	11950 to 12789
2.00	13627	2024	14.8	12679 to 14574

Figure 17. Dynamic fatigue of abraded fused quartz
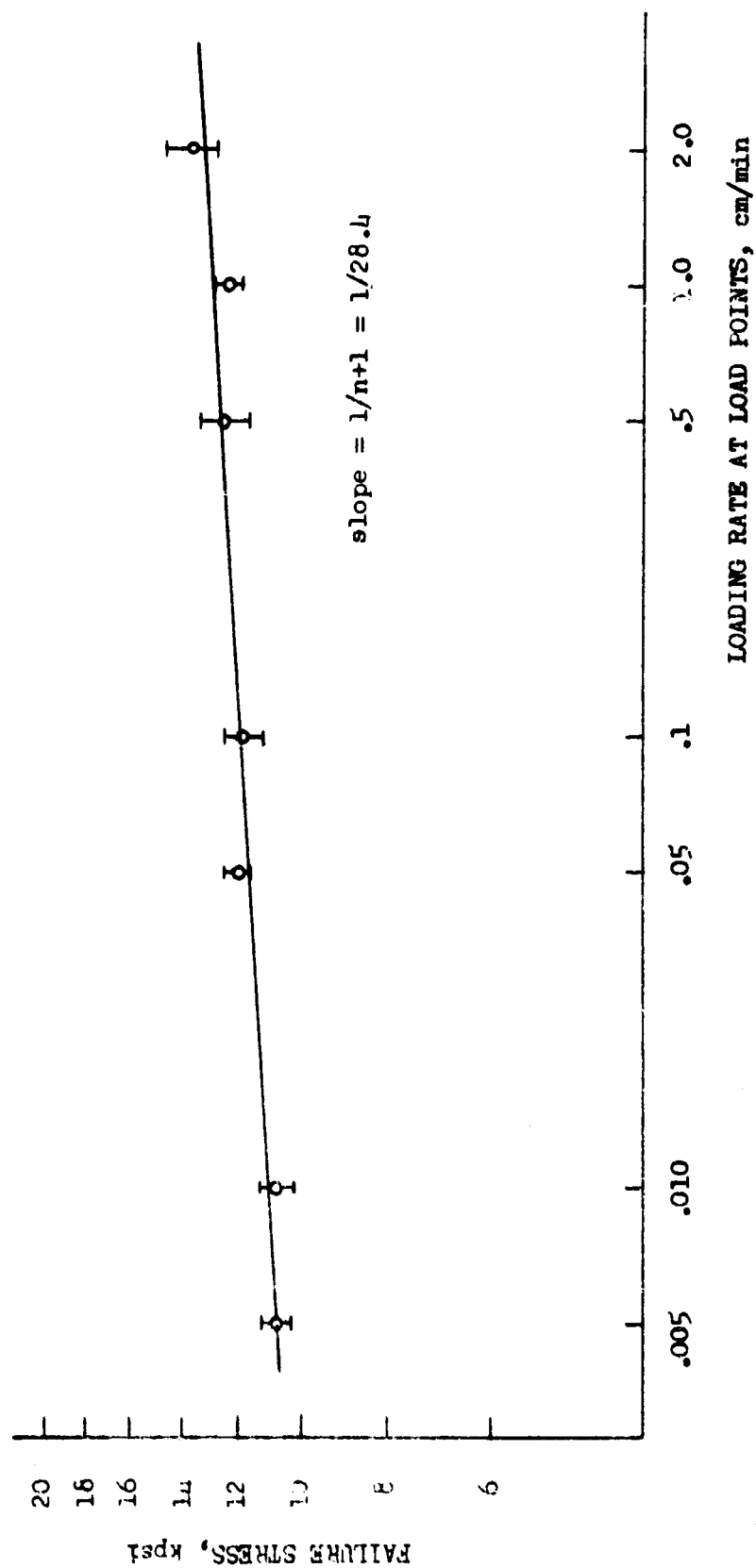
Figure 18. Dynamic fatigue of abraded pyrex

12.0 DISCUSSION-STATIC AND DYNAMIC FATIGUE OF SILICATE GL SES

12.1 Dynamic Fatigue

To describe flaw growth under dynamic conditions Charles[3] assumed that

$$v_x = K \sigma_m^n \qquad (1)$$

where v_x is the velocity of the flaw tip in the direction, σ_m is the normal tensile stress at the flaw tip, and k, n are constants. He then derived, Eqn. (2), that "n" may be experimentally evaluated from the slope of a log-log plot of failure stress versus loading rate. The results of various investigators are given in Table 9A.

Wiederhorn[9,10] using the crack velocity equation developed from reaction rate theory by Charles and Hillig[5] derived that

$$v = v_o \exp - (E^* - bK_1)/RT \qquad (6)$$

where v is the crack velocity and v_o, E^* and b are parameters which may be experimentally evaluated by fitting crack velocity data to the above equation. K_1 is the stress intensity factor, proportioned to stresses at the crack tip.

It would be of extreme importance to be able to relate the fundamentally derived parameters E^* and b from Wiederhorn's crack velocity equation to the empirical constant "n" determined from measuring fracture strength as a function of stress-rate. however, the analytical condition is not known at present (see Appendix B).

TABLE 9

Comparison of Crack Velocity and Dynamic Fatigue Data

A. Dynamic fatigue data

Glass	Surface cond.	Reference	"n"
Soda-lime (Kimble R-6)	acid-etched	Ritter[6]	13.0
Soda-lime (Corning 0080)	abraded	Charles[3]	16.0
E-glass*	pristine fiber	Cameron[16]	27.0
Fused quartz (Gen. Elect.)	abraded	This inv.	37.8
Pyrex (Corning 7740)	abraded	This inv.	27.4

B. "n" Determined from crack velocity measurements of Wiederhorn[10]

Glass	"n"
Soda-lime (Libby-Owens Ford)	16.6
Aluminosilicate**(Corning 1720)	27.4
Fused silica (Corning 7940)	36.1
Pyrex (Corning 7740)	34.1

* E-glass has nominal composition, weight percent 54.4 SiO_2, 14.4 Al_2O_3, 17.5 CaO, 4.5 MgO, 8.0 B_2O_3, 0.5 Na_2O + K_2O, 0.4 Fe_2O_3, 0.3 F_2.[30]

** This has nominal composition, weight percent 57.0 SiO_2, 20.0 Al_2O_3, 6.0 CaO, 12.0 MgO, 4.0 B_2O_3, 1.0 Na_2O, which is very similar to E-glass.

Instead crack velocity measurements may still be correlated with dynamic fatigue data since the theory of Charles[3] assumes that a plot of log v versus log K_I should be a straight line with the slope giving "n". This has been done using Wiederhorn's[10] experimentally determined stress corrosion constants and the results are given in Table 9b.[29] The fit of the velocity-stress intensity data to a log-log plot was very good, especially at the high velocity end.

Comparisons of "n" values computed from dynamic fatigue tests and "n" values determined from the crack velocity data of Wiederhorn agree well on both a qualitative and quantitative level. The largest discrepancy was for pyrex glass, 27.4 versus 34.1, and these measurements are currently being checked.

12.2 Static Fatigue

Static fatigue curves for acid-etched, soda-lime-silica glass at $74°$ F and 50% and 100% relative humidity, Fig. 15, are very nearly parallel. The breaking stress decreases at approximately 14,500 psi per log decade of time and breaking stresses at 50% relative humidity are 17% higher than those at 100% relative humidity. This correlates with the work of Otto[19] who tested fibers of various silicate glasses in dry air having $-13°$ F dewpoint and in air at 50% relative humidity. Otto's static fatigue tests showed breaking stress decreased at 15,000 to 20,000 psi per log decade of time regardless of temperature or ambient humidity. He also found that in static fatigue tests at room temperature breaking stresses were generally 10% higher in dry air than at 50% relative humidity.

Static results for acid-etched soda-lime-silica glass may
be normalized in the reduced units of the universal fatigue curve
of Mould and Southwick. This has been done for the 100% relative
humidity results in Section 10.2. The same procedure may be used
for the 50% relative humidity results and from Figure 15 the correspond-
ing value of $t_{0.5}$ is 0.148 minutes. Using these values the slope of
the reduced curve is -.031. The intercept is 0.5 as it must be for
any universal fatigue curve. Comparison of these results with those
of Section 10.2 shows that the static fatigue of acid-etched, soda-
lime-silica glass at 74°F and 50% and 100% relative humidity may
be represented by a single universal fatigue curve. This curve and
the reduced data points at both humidities is shown in Fig. 19.
This agrees with Wiederhorn's[10] formulation of the universal fatigue
curve, Eqn. 8, which predicts that a universal fatigue curve is
independent of relative humidity. A slight rearrangement (Eqn. 9)
of Wiederhorn's formulation of the universal curve fatigue also
shows that static fatigue curves determined for a given chemical
composition and temperature but at different relative humidities
should be parallel as in Fig. 15 when presented in the usual manner
(failure stress vs log time to failure).

Universal fatigue curves may also be determined for E-glass
and fused silica. Data presented in Fig. 3 on static fatigue of
E-glass and in Fig. 4 for fused silica were read by the present
author from plots in publications of the investigators listed.
A similar procedure to that for acid-etched, soda-lime-silica glass
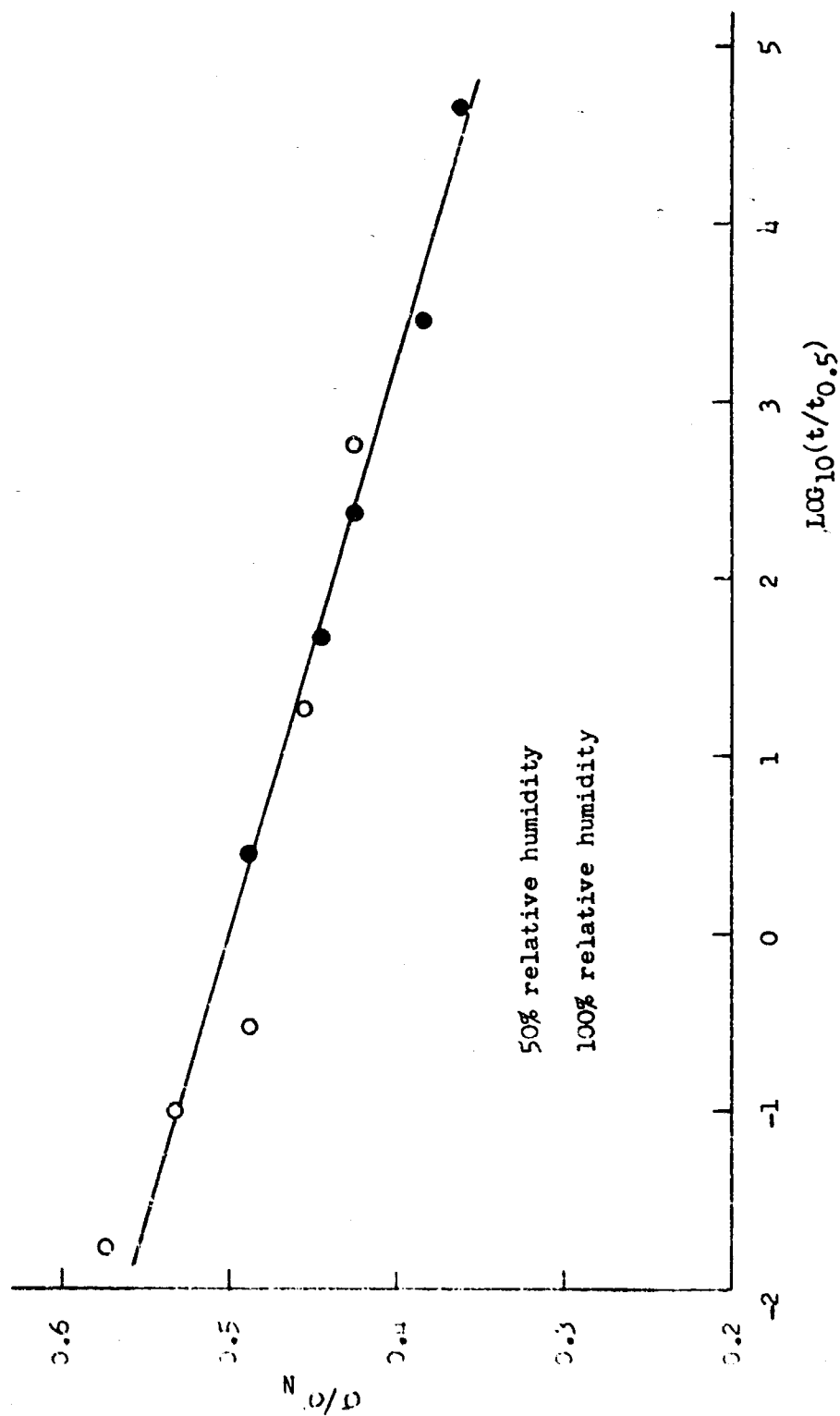was then used to obtain the universal fatigue curves. Proctor's[23]

Figure 19. Universal static fatigue curve of acid-etched,
soda-lime-silica glass at $74°F$

data for samples tested in liquid nitrogen showed a median failure stress of approximately 1200 kg/mm^2. The corresponding $t_{0.5}$ from Fig. 4 equals 0.122 seconds. Using these values the slope of the universal fatigue curve for fused silica is -.041. The universal fatigue curve for E-glass was determined using the curve in Fig. 3 marked Hollinger et al.[20]. This curve was chosen since it represents the median curve of the three investigators of static fatigue in E-glass. Cameron[18] has measured σ_N equal to 820,000 psi for E-glass fibers. From Fig. 3 the corresponding value of $t_{0.5}$ is 28.2 seconds. Using these values the slope of the universal fatigue curve for glass is -.036.

Universal static fatigue curves as determined above for various silicate glasses are shown for comparison in Fig. 20. Surprisingly, Fig. 20 shows little if any difference in susceptibility to static fatigue among the three high strength silicate glasses despite differences in chemical composition. This is in contrast to the results of dynamic tests (Section 12.1). A possible explanation for this lies in the difference of crack size for high and low strength glasses. Charles[4] has noted that dissolution of multi-component silicate glasses, fused silica, and quartz is greatly enhanced in basic solutions. He also showed that corrosion of unstressed soda-lime-silica glass occurs more rapidly in steam than in water at the same temperature because great dilution is possible in water and therefore pH buildup is slower than in the corrosion products of a like sample in steam. Wiederhorn[31] has recently suggested that the effect of glass composition on corrosion is to
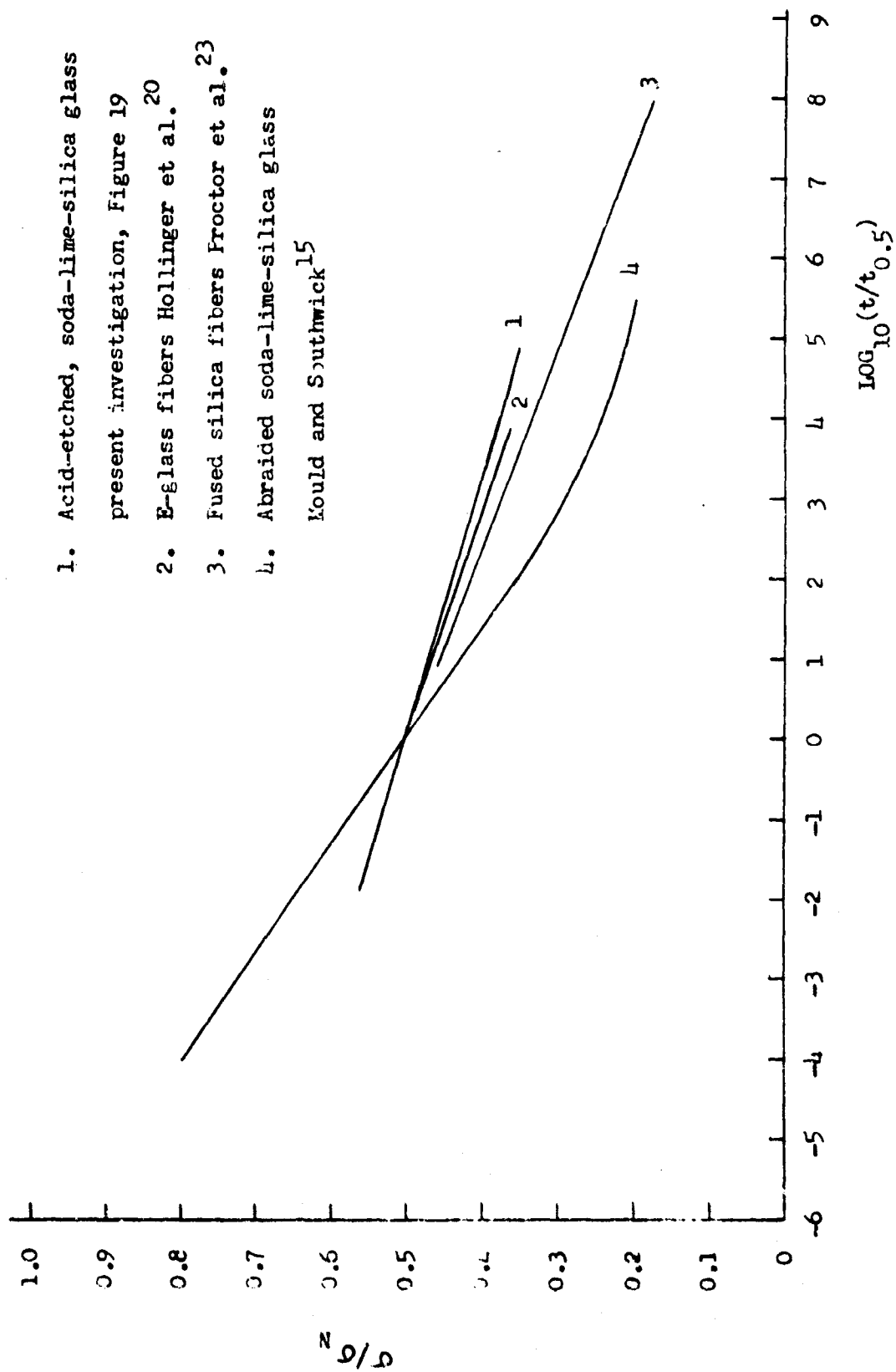
Figure 20. Static fatigue of silicate glasses

control the pH at the tip of the crack. One would reasonably
expect that the control of pH would be more effective in deep cracks
than in the relatively shallow cracks that would be present in
high strength glass. The expansion of corrosion products would
also retard entrance of bulk water to the interior of a deep crack.
Thus one might expect to see little effect of glass composition
on the static fatigue of high strength glasses. However, this does
not explain Ritter's[6] results that dynamic tests of both high and
low strength soda-lime-silica glass predict the same fatigue sus-
ceptibility. To resolve these questions, additional static fatigue
tests of low strength silicate glasses of differing chemical com-
positions are required to further elucidate the effect of chemical
composition on static fatigue. Further attention must also be
given to the specific kinetic processes occurring during corrosion
at a crack in a glass surface.

13.0 CONCLUSIONS

(i) Dynamic fatigue data can be compared to fundamental crack velocity data utilizing Charles' dynamic fatigue theory. Agreement is good on both a qualitative and quantitative level for a wide variety of silicate glasses.

(ii) The static fatigue data for acid-etched, soda-lime-silica glass does not lie on the universal fatigue curve of Mould and Southwick determined for abraded soda-lime-silica glass. The acid-etched glass was less susceptible to static fatigue than the abraded glass.

(iii) Static fatigue curves of acid-etched, soda-lime-silica glass determined at 74° F in atmospheres of 50 and 100% relative humidity can be represented by a single universal fatigue curve. These results are in agreement with the predictions of Wiederhorn on the influence of relative humidity on the static fatigue curve.

(iv) There is little difference in the static fatigue susceptibility, as measured from a universal fatigue curve, of high strength silicate glasses (soda-lime, E-glass, and fused silica). This could be due to the nature of the surface crack on these high strength glasses being relatively shallow which would allow the corrosion products being diluted by the surrounding water so that the glass composition has little effect on the pH at the crack tip.

14.0 FUTURE WORK

To further elucidate the effect of composition on low strength silicate glasses, the static fatigue curves of abraded pyrex and fused silica should be determined. Once the effect of composition on the static fatigue of low strength silicate glasses is understood, these results can be compared with those of the present study for high strength silicate glasses. Present fatigue theory should be revised to account for the dependence of fatigue susceptibility on chemical composition and for the different high and low strength behavior. Also, further attention must be given to the specific kinetic processes occurring during corrosion at a crack in the surface of a silicate glass.

REFERENCES

1. R. E. Mould, "The Strength of Inorganic Glass," in Fundamental Phenomena in the Materials Sciences, Vol. 4, Plenum Press, 119-149 (1967).

2. J. E. Ritter, Jr., "Glass-Material for Deep-Sea Submersible Vehicles," Glass Ind., 49, 603-608 (1968).

3. R. J. Charles, "Dynamic Fatigue in Glass," J. Appl. Phyc., 29, 1657-1662 (1958).

4. R. J. Charles, "Static Fatigue of Glass, I-II," J. Appl. Phys., 29, 1949-1560 (1958).

5. W. B. Hillig and R. J. Charles, "Surfaces, Stress-Dependent Surface Reactions and Strength," in High Strength Materials, Ed. V. F. Zackey, John Wiley and Sons, Inc., New York (1965).

6. J. E. Ritter, Jr., "Dynamic Fatigue of Soda-Lime-Silica Glass," J. Appl. Phys., 40, 340-344 (1969).

7. L. Holland, The Properties of Glass Surfaces, John Wiley and Sons, Inc., New York (1964).

8. M. Watanabe, R. V. Caporali, and R. E. Mould, "The Effect of Chemical Composition on the Strength and Static Fatigue of Soda-Lime Glass," Phys. and Chem. of Glasses, 3, 7-27 (1962).

9. S. M. Wiederhorn, "Influence of Water Vapor on Crack Propagation in Soda-Lime Glass," J. Am. Ceram. Soc., 50, 407-414 (1967).

10. S. M. Wiederhorn and L. H. Bolz, "Stress Corrosion and Static Fatigue of Glass", J. Am. Ceram. Soc., 53 (10), 543-48 (1970).

11. R. J. Charles, pp. 1-38 in Progress in Ceramic Science, Vol.1. Edited by J. E. Burke, Pergammon Press, New York, 1961.

12. W. B. Hillig, pp. 152-194 in Modern Aspects of the Vitreous State, Vol. 2. Edited by J. D. Mackenzie, Butterworth Inc., Washington, D. C., 1962.

13. A. A. Griffith, "Phenomenon of Rupture and Flow in Solids," Phil. Trans Roy. Soc. (London), 221a, 163 (1920).

14. E. Orowan, "Energy Criteria of Fracture, "Welding J., 34 157S-160S (1955).

15. R. E. Mould and R. D. Southwick, "Strength and Static Fatigue of Abraded Glass Under Controlled Ambrient Conditions, "Part 1," J. Am. Ceram. Soc., 42, 542-547 (1959); "Part II," ibid., 42, 542-547 (1959); "Part III," ibid., 43, 160-167 (1960); "Part IV," ibid., 44, 481-491 (1961).

16. E. B. Shand, "Experimental Study of Fracture of Glass: I, Fracture Process, "J. Am. Ceram. Soc., 37, 52-60 (1954); "II Experimental Data," ibid., 559-572 (1954).

17. C. J. Phillips "Strength and Weakness of Brittle Materials," Am. Scientist, 53, 20-51 (1965).

18. N. M. Cameron, "The Effect of Environmental Treatments on the Strength of E-Glass Fibers," T and AM Report No. 274, University of Illinois, under U. S. Bureau of Naval Weapons Contract NOW 64-0178-d (1966).

19. W. H. Otto, "The Effects of Moisture on the Strength of Glass Fibers--A Literature Review," Whittaker Corp., under U. S. Naval Research Laboratory Contract Nonr 4522(00) (x) (1965).

20. D. L. Hollinger, W. G. Kanetzky, and H. T. Plant, "Influence of Stress Corrosion on Strength of Glass Fibers," Fourth Bi Monthly Progress Report on U. S. Naval Research Laboratory Contract No. Nonr 4486(00) (x), General Electric Company 1964.

21. G. K. Schmitz and A. G. Metcalfe, "Stress Corrosion of E-Glass Fibers," Ind. Eng. Chem. Prod. Res. Dev., 5, 1-8 (1966).

22. J. G. Morley, P. A. Andrews and I. Whitney, "Strength of Fused Silica," Phys. and Chem. Glasses, 5, 1-10 (1964).

23. B. A. Proctor, I. Whitney, and J. W. Johnson, "The Strength of Fused Silica," Proc. Roy. Soc., 297a, 534-557 (1967).

24. B. Proctor, "The Effects of Hydrofluoric Acid Etching on the Strength of Glasses," Phys. and Chem. Glasses, 3, 7-27 (1962).

25. D. L. Vrooman and J. E. Ritter, "Nonlinear Behavior of Thin Beams in Four Point Bending," Am. Ceram. Soc. Bull., 49, 789-93 (1970).

26. R. V. Caporali, "Melting History Effects on the Strength of Lithium-Potassium and Lithium-Sodium Silicate Glass Systems," Pennsylvania State University, Dept. of Mat. Sci. (1969).

27. J. E. Ritter and D. L. Vrooman, "Static Fatigue of Acid-Etched Soda-Lime-Silica Glass Rods," Project Themis Report No Themis-UM-69-4 University of Massachusetts under Office of Naval Research Contract No. N0014-68-A-0146 (1969).

28. J. E. Ritter and A. R. Cooper, Jr., "The Fracture Strength of Commercial Soda-Lime-Silica Glass from -100 to 700 C," Phys. and Chem. Glasses, $\underline{4}$, 76-78 (1963).

29. S. M. Wiederhorn, private communication, Oct. 1970.

30. R. E. Lowrie, p.280 in Modern Composite Materials, Edited by L. J. Broutman and R. H. Krock, Addison-Wesley, Reading, Mass., (1967).

31. S. M. Wiederhorn, talk at 72nd Annual Meeting American Ceramic Society, Philadelphia, May 1970. Abstract Given in Bull. Am. Ceram. Soc., $\underline{49}$ (4) (1970).

32. C. E. Inglis, "Stresses in a Plate Due to the Presence of Cracks and Sharp Corners," Trans. Inst. Naval Arch., $\underline{55}$, 219-230 (1913).

APPENDIX A   SAMPLE CALCULATIONS

The slope of the static fatigue curve in reduced units given by Charles and Hillig[5] is:

$$\frac{d \ln t}{d(\sigma/\sigma_N)} = \frac{V^* \sigma_u}{RT}$$

Substituting the values of temperature, T, of 296°K and the slope of -74.2 for the static fatigue data, and assuming a theoretical strength for soda-lime-silica glass of 2.0×10^6 psi or 1.38×10^{11} dynes/cm^2, the following equation is obtained:

$$\frac{d \ln t}{d(\sigma/\sigma_N)} = -74.2 = \frac{-V^* (1.38 \times 10^{11} \text{dynes/cm}^2)}{(8.313 \times 10^7 \text{dyne-cm/gmol K})(296^\circ\text{K})}$$

The value of V^*, the activation volume for alkali metal ion diffusion in the glass is found to be $V^* = 13.2$ cm^3/mole.

Γ/L from Eqn. 4 is:

$$\frac{\Gamma}{L} = \frac{8 V^* S_L^2}{3 \sigma_{th} V_m}$$

By substituting the value of the fatigue limit stress, S_L, of 1.5×10^5 psi or 1.03×10^{10} dynes/cm^2, assuming a value of the molar volume, V_m, of 20 cm^3, and using the above values of σ_u and V^*, the ratio Γ/L can be calculated.

$$\frac{\Gamma}{L} = \frac{8 \times 1.32 \times 10^1 cm^3/gmol \times 1.06 \times 10^2 dynes^2/cm^4}{3 \times 1.38 \times 10^{11} dynes/cm^2 \times 2 \times 10^1 cm^3/gmol}$$

$$\frac{\Gamma}{L} = 1.355 \times 10^9 \text{ dynes/cm}^2 = 1.355 \times 10^9 \text{ ergs/cm}^3$$

By using the Orowan[14] criteria of fracture:

$$\frac{\sigma_u}{\sigma} = 2\left[\frac{L}{\rho}\right]^{\frac{1}{2}}$$

with $\sigma_u = 2.0 \times 10^6$ psi, $\sigma = 2.0 \times 10^5$ psi and $\rho = 2.5 \times 10^{-8}$ cm, the crack depth, L, equals 6.25×10^{-7} cm. Using this value of L the value of Γ, the surface free energy between the solid and the reaction product, can be calculated to be 846 dynes/cm^2.

APPENDIX B RELATIONSHIP OF FAILURE STRESS TO STRESSING RATE

An attempt was made to relate failure stress to stressing rate using Wiederhorn's[9,10] fundamental crack velocity expression (Eqn. 6) following the general method employed by Charles.[3] Eqn. 6 may be rewritten as

$$v = v_c \exp - (E* - B\sigma_m)/kT$$

Where v is the crack velocity and σ_m is the normal tensile stress at the crack tip. v_c, $E*$ and B are parameters which may be experimentally evaluated by fitting crack velocity data.

Inglis[32] has shown that

$$\sigma_m = 2 \sigma_a (x/\rho)^{\frac{1}{2}}$$

Where σ_a is the macroscopic applied stress, X is the depth of the crack and ρ is the radius of curvature of the crack tip. ρ is of interatomic dimensions and may be assumed constant during crack growth. Similarly Orowan[14] using Griffith's results has shown that

$$\sigma_{cr} = 2 \sigma_{af} (X_{cr}/\rho)^{\frac{1}{2}}$$

Where σ_{cr} is the theoretical strength of the material in tension, σ_{af} is the macroscopic applied stress at which failure occurs and X_{cr} is the critical flaw depth for spontaneous crack propagation.

In a dynamic test the applied stress may be expressed most simply as

$$\sigma_a = \beta t$$

Where t is time and β is stressing rate. Also

$$\sigma_{af} = \beta t_f$$

Where σ_{af} is the macroscopic applied stress at which failure occurs, as previously defined, and t_f is the time to failure. Therefore,

$$\sigma_E = 2\beta t (X/\rho)^{\frac{1}{2}}$$

Substituting the above equation into the velocity equation we obtain

$$v_x = dx/dt = v_0 \exp - \left[(E^* - 2U\beta t (X/\rho)^{\frac{1}{2}})/RT \right]$$

This is a nonlinear differential equation and an analytical solution is not known at present.

DOCUMENT CONTROL DATA - R & D		
Security classification of title, body of abstract and indexing annotation must be entered when the overall report is classified)		
1. ORIGINATING ACTIVITY (Corporate author) School of Engineering University of Massachusetts Amherst, Massachusetts 01002	2a. REPORT SECURITY CLASSIFICATION UNCLASSIFIED 2b. GROUP	

3. REPORT TITLE

DYNAMIC AND STATIC FATIGUE OF SILICATE GLASSES

4. DESCRIPTIVE NOTES (Type of report and inclusive dates)

5. AUTHOR(S) (First name, middle initial, last name)

John E. Ritter, Jr. and Charles L. Sherburne

6. REPORT DATE December 1970	7a. TOTAL NO. OF PAGES 84 + ix	7b. NO. OF REFS 32
8a. CONTRACT OR GRANT NO ONR-N00014-68-A-0146 b. PROJECT NO. In-house Project Number cN00014-68-A-0146-3 d.	9a. ORIGINATOR'S REPORT NUMBER(S) UM-70-9 9b. OTHER REPORT NO(S) (Any other numbers that may be assigned this report)	

10. DISTRIBUTION STATEMENT

Distribution of this document is unlimited

11. SUPPLEMENTARY NOTES	12. SPONSORING MILITARY ACTIVITY Department of Defense (ONR)

13. ABSTRACT

Fatigue of silicate glasses was studied using both static and dynamic tests. Static fatigue data for acid-etched, soda-lime-silica glass determined at 74° F in atmospheres of 50 and 100% relative humidity could be represented by a single universal fatigue curve. The UFC for acid-etched glass does not lie on the UFC of Mould and Southwick which was determined for abraded soda-lime-silica glass, the acid-etched glass being less susceptible to static fatigue. On comparing the fatigue behavior of acid-etched, soda-lime-silica glass to that of pristine E-glass and fused silica fibers, little difference was found in the susceptibility to static fatigue. In addition, dynamic fatigue data for a wide variety of silicate glasses (soda-lime-silica, E-glass, pyrex, and fused quartz) was compared to fundamental crack velocity data for these glasses utilizing the dynamic fatigue theory of Charles. Agreement was good on both a quantitative and qualitative level. The theoretical implications of these results on static and dynamic fatigue are discussed.

14 KEY WORDS	LINK A		LINK D		LINK C	
	ROLE	WT	ROLE	WT	ROLE	WT
Static Fatigue						
Dynamic Fatigue						
Silicate Glasses						
Stress Corrosion Susceptibility						